AIR FORCE INSTITUTE OF TECHNOLOGY

AIR UNIVERSITY
UNITED STATES AIR FORCE

SCHOOL OF ENGINEERING

WRIGHT–PATTERSON AIR FORCE BASE, OHIO

AF-WP-O-MAY 62 3,500

ION PRODUCTION AND FLOW IN AN ELECTROHYDRODYNAMIC GENERATOR

Terry N. Lauritsen

GA/ME/62-3

AF-WP-O-SEP 62 25

ION PRODUCTION AND FLOW IN AN ELECTROHYDRODYNAMIC GENERATOR

THESIS

Presented to the Faculty of the School of Engineering of
the Air Force Institute of Technology
Air University
in Partial Fulfillment of the
Requirements for the Degree of
Master of Science

by

Terry N. Lauritsen, B.S.
1/Lt USAF
Graduate Astronautics

August 1962

Preface

I was first introduced to the field of electrohydrodynamics by Dr. Hans Von Ohain, of the Aeronautical Research Laboratory, during his presentation of thesis topics to students of the Air Force Institute of Technology. Since then, it has been a great pleasure for me to work with the subject and with him.

The purpose of this thesis is to present the characteristics of ion production and flow in an electrohydrodynamic generator which was designed and built, in nearly its present configuration, by the Aeronautical Research Laboratory. Much of my work toward that end, however, consisted of acquiring and setting up suitable instrumentation and test equipment. The overall approach I used was almost entirely experimental and practical: ideas and methods which did not work were discarded, and alternate ones were tried. This led, finally, to the results presented herein.

I wish to gratefully acknowledge the guidance and help of Dr. Von Ohain and my thesis advisor, Major Hamilton. Mr. David Murray of the Aeronautical Research Laboratory, busy as he was, could always be called upon for assistance, and Mr. Jack McClary was very cooperative in providing the high pressure air supply. Captain H. P. Wheeler, Jr., with whom I shared the apparatus, was extremely helpful in all ways, and it would have been impossible to conduct the experimental procedure without him. I would also like to thank my wife for her understanding, patience, and help during the many hectic days of manuscript preparation.

Terry N. Lauritsen

Contents

Contents

List of Figures

List of Figures

List of Tables

List of Tables

List of Symbols

Symbol	Definition	Units
A	Area	in.^{2} or m^2
E	Electric field intensity	volts/m
I	Electric current	amps, ma, or µa
K	Ion mobility at standard T and P	m^2/volt-sec
L	Length of transport region	in.
M	Mach number	none
N	Ion concentration	ions/cm^3
P	Pressure	psig or psia
T	Temperature	^{o}F or ^{o}R
V	Electric potential	volts or kv
e_o	Permittivity of free space	farad/m
k	Ion mobility	m^2/volt-sec
$\dot{m}$	Mass flow rate	lbm/sec
r	Radius	in. or m
r_o	Assumed radius of grounded wire	m
u	Ion velocity relative to gas	m/sec
v	Gas velocity	ft/sec or m/sec
x	Axial coordinate in nozzle	in. or m
ρ	Gas density	lbm/ft^3
ρ_e	Electric charge density	coul/m^3

List of Symbols

Symbol	Definition	Units

Subscripts

0	Reservoir conditions	
1	Nozzle throat	
2	Needle point	
3	Nozzle exit	
4	Transport region	
5	Ion collector screen	
6	Body of ion collector	
a	attractor plate electrode	
avg	average	
c	Collector electrode	
esc	Escape	
gp	Ground plate electrode	
i	Initial	
n	Needle electrode	
r	Radial	
s	Standard conditions	
x	Arbitrary station in nozzle	

Abstract

Electrohydrodynamic (EHD) power generation is a process for converting dynamic energy of a flowing fluid directly into electrical power. It differs from magnetohydrodynamics in that only externally applied electric fields are used to interact with the fluid. An experimental EHD generator was built by the Aeronautical Research Laboratory of the Office of Aerospace Research, USAF. It used air for the working fluid, and partially ionised it through the use of multiple corona discharge needles. The objective of this study was to determine the characteristics and trends of ion production and flow in that generator.

The experimental apparatus consisted of the cylindrical EHD generator itself (4-1/2 inches in diameter, 5 inches long), a high voltage source for the corona discharge, and instrumentation. The geometry of the ionization region of the generator was variable: ten different configurations were evaluated for their current-producing capability. In addition, the most favorable configuration was further investigated in regard to the effects of air density, distance of ion transport, and polarity of the ions.

The results of the experimentation showed that the generator was successful in accomplishing EHD power conversion. Currents on the order of 500 microamperes were produced when an air supply pressure of 200 psig was used. The most favorable ionization

configuration was found to be the one in which each grounded needle point was axially (and, of course, radially) centered within a high potential circular electrode. The air density, or total pressure, was the prime factor in determining the magnitude of current which could be produced. A distance of ion transport of more than half an inch had a detrimental effect on the output current, but a grounded electrode between the ionization and transport regions shielded the corona needles from this effect. The generator was able to produce ion currents of either polarity, although its performance was better with the negative ions.

This study showed that EHD conversion of fluid flow energy to electrical power is possible, and that multiple needle corona discharge is a practical method of ionization for the process.

Further investigation of EHD power conversion, and further improvement and testing of the generator used in this study, are recommended.

ION PRODUCTION AND FLOW IN AN ELECTROHYDRODYNAMIC GENERATOR

I. Introduction

Background

Conversion of energy from one form to another is a familiar, necessary process. Of the many different conversions that are accomplished, perhaps the most common is that from the thermal energy of a gas to electrical power. This process, as accomplished in modern fossil fuel power stations, has an efficiency of only about 35% (Ref 5:1), with large losses occurring in the turbine element. This has led to much effort toward obtaining a more direct energy conversion process: one that would bypass mechanical energy, and thereby eliminate the need for a conventional turbine and generator. Aside from the possible gain in efficiency, the elimination of the turbine and generator in such a process would likely result in lighter equipment. This would be a particular advantage in a system to be used on space missions.

Two approaches presently being studied are magnetohydrodynamics (MHD) and electrohydrodynamics (EHD). The first of these involves interaction of partially ionized flowing fluids with externally applied magnetic fields, and results in charge separation and electrical output. The other approach, EHD, also uses a partially ionized flowing fluid, but the necessary charge separation is accomplished through the use of externally applied electric fields only. There are considerations and problem areas common to both processes, as well as significant differences between them. Good discussions and comparisons can be found in References 5 and 9, pages 1-7 and 102-104, respectively. Since this report deals with EHD exclusively, no attempt has been made to include in the bibliography any of the large number of possible references on MHD alone. The field of EHD has received much less study (because it has appeared to be less promising), and a fairly comprehensive list of references can be given:

A broad discussion of possible electrostatic interactions is presented in Reference 12, and several other sources outline well the theoretical work that has been done specifically concerning EHD power generation (Refs 4, 6, 10, and 11).

The experimental work that has been done is limited. Stuetzer, of General Mills, has conducted what is probably the most extensive test program to date, using various liquids as the working fluid (Ref 11). Very limited investigations of gaseous working fluids have been made by Gourdine (Ref 4:5), Petruzzella (Ref 7), and Smith (Ref 9:74-84), all of whom used a single free stream of atmospheric air.

Other related theoretical and experimental work includes that on the corona discharge mechanism (Ref 13:1-28), which can be used for the necessary ionization; and on the "electric wind" (Ref 8), which is essentially the reverse of EHD power generation as discussed in this report.

Electrohydrodynamic Power Generation

The basic principle of an EHD generator is physical separation of electric charge. The operation is very similar to that of a Van de Graff generator, except that the charge is moved by the action of a fluid rather than by a solid belt. Figure 1 is a simple illustration of the process. (In this report, all figures are grouped together in Appendix A, which begins on page 38.) A neutral fluid flowing through an insulating channel is partially ionized, or has ions injected into it, at the plane of ionization. This is done in such a way that ions of one sign only are permitted to be swept through the transport region by the action of the fluid. The charges are thus separated, and a potential difference builds up. When the ions reach the plane of neutralization, the conducting path through the load resistor allows neutralization to occur. That is, while the <u>ions</u> are formed and carried through the channel, <u>electrons</u> flow through the external load circuit to neutralize them again. Of course, in practice, both ionization and neutralization must take place over a finite distance, and aerodynamic losses must be minimized by proper design of the entire flow channel.

One of the necessary conditions for the achievement of an acceptable output voltage by the EHD generation process is that energy be transferred from the large number of neutral fluid particles to the relatively few charged particles in the flow (Ref 6:8). There are two possible methods for accomplishing this. One, as implied by Figure 1, is to use the viscous interaction between the fluid molecules and the ions, with the coupling of momentum and energy resulting from collisions of the particles. (It is apparent that there is some slippage in this case, as the electric field in the transport region pulls back on the charged particles. This will be described later through the concept of "mobility".) The other method of coupling is to convert the available energy of the fluid medium into kinetic energy of high speed charged droplets (particles larger than ions) which then are allowed to follow a ballistic path through a similar transport region. An excellent discussion of these two types of EHD coupling processes can be found in the work by Lawson et al. (Ref 6:8-9, 14-23).

An area of fundamental importance in the successful operation of an EHD generator, and one which is usually neglected in theoretical studies (Refs 3:2, 4:1, 10:1), is the method of obtaining the charged particles in the fluid flow. Several possibilities which have been considered are as follows:

a. Radiation
b. Thermal ionization
c. Surface contact ionization
d. Direct injection of particles
e. Action of electric fields

Of these, the action of an electric field, or corona discharge, has been the method used for the published experimentation to date, and was the method used in the work covered by this thesis. In fact, determination of the feasibility and characteristics of this method of ionization were a major part of the study, as indicated below.

Objective of the Study

During 1960 and 1961, under the authority and documentation of Project No. 7116-03, the Aeronautical Research Laboratory of the Office of Aerospace Research, USAF, designed and built a prototype electrohydrodynamic generator. The design, based both on theoretical work (Refs 3, 4, and 6) and on preliminary experimental findings of N. L. Petruzzella (Ref 7), specified air as the working fluid, incorporated a multiple electrode corona discharge arrangement for the source of ionization, and allowed for various changes of geometry. The purpose of this study was to determine, as completely as possible, the characteristics and trends of ion production and flow in that generator.

Another study (Ref 14), conducted concurrently with this one, evaluated the volt-ampere, or power, characteristics of the same generator.

II. Description of Apparatus

The experimental apparatus, two overall views of which are presented in Figure 2, consisted of the EHD generator itself, and various other equipment for its operation. These will be described in turn.

The Electrohydrodynamic Generator

An EHD generator is a flow-through device for obtaining electrical power directly from the dynamic energy of a moving fluid. The basic principle of operation has already been illustrated in Figure 1.

Overall Description. As has been previously stated, the generator studied for this thesis used air as the working fluid, and ionized it by the corona discharge method. The unit was cylindrical, with outside dimensions of 4-1/2 inches (diameter) by 5 inches (length). It was made of plexiglass and steel, with its several disk-like sections held together by a peripheral circle of sixteen 5/16-inch bolts. Figure 3 shows two external views of the generator. The internal flow channel varied from about 0.3 to 1.0 square inch. Figure 4 is a full size sectional side view, and Appendix B contains a complete set of engineering drawings for the device.

The principle areas of interest within the generator were the ionization region, the transport region, and the neutralization region. These are further described on the following pages.

Ionization Region. The region where ion formation occurred was of foremost importance in the study. It was a composite region, consisting of 25 parallel convergent-divergent plexiglass nozzles arranged in a square. Centered in each nozzle was a sharp needle electrode. The other electrode (the "attractor plate") for producing the necessary corona was around the circumference of each nozzle as can be seen, in one of its two possible locations, in Figure 4 (Item 5). An actual attractor plate, attached to the exit plane of a plastic nozzle disk (the other possible location), and partially coated with insulating lacquer, is shown in Figure 5.

The geometry of the ionization region was a primary variable in the study. In all cases, the nozzles themselves remained the same, each of them having an exit diameter of 0.147 inch, a throat diameter of 0.125 inch (with the throat area further reduced by the needle shaft), and an expansion half angle of 3°. Two locations for the steel attractor plate were possible, however (compare Figures 4 and 5), and the axial coordinate of the needle points was variable. (The position of the needle points was determined by plastic spacers, which are Item 3 in Figure 4, and which are shown separately in Figure 6.) In all, ten different configurations of the ionization region were selected for study. They are shown, with pertinent dimensions, in Figure 7. It also can be seen from Figure 7 that when the attractor plate was located in mid-nozzle, an essentially identical "ground plate" was used at the nozzle exit to act as a shield between the ionization region and the transport region. Table I gives all appropriate areas and area ratios for the nozzles, individually and collectively, and for the transport and neutralization regions as well. (Tables I-IV are in Appendix A, pages 65-68.)

Transport Region. The transport region (Item 9, Figure 4) was a single one-inch-square channel of variable length (zero to one inch) having plexiglass sides. It was bounded on the upstream end by either the ground plate (Configurations IV-X) or the attractor plate (Configurations I-III), and on the other end by the ion collector (see below). For most of the work discussed in this thesis the length of the transport region was one-half inch.

Neutralization Region. Neutralization of the ions took place in the "collector" electrode, two views of which are shown in Figure 8. The electrode was a steel gridwork that was held in position in the flow channel by four setscrews (Item 8, Figure 4), allowing the length of the transport region to be varied as mentioned above. The collector was 2.25 inches long, with the internal grid breaking the flow channel into 25 sections that had length-to-diameter ratios of approximately 10. A stainless steel screen was soldered on the upstream end to act as an effective end plane for the field lines in the transport region. The available flow area through this screen is shown as station 5 in Table I, and the main part of the collector is station 6.

Other Equipment

A complete schematic diagram of the experimental equipment is given in Figure 9, and Figure 10 is a photograph of the power supply and electrical instrumentation.

<u>High Voltage Power Supply</u>. The ionizing potential to the attractor plate was provided by a "Beta Series 201 Portable High Voltage D.C. Power Supply". It was capable of supplying 0-30,000 volts at a maximum current of 1 ma, and could be wired for either positive or negative polarity. It was found necessary to isolate the power supply from building ground by use of the isolation transformer shown in the schematic diagram. The 30-megohm resistance in series with the supply was protection against a short circuit or severe sparkover in the EHD generator.

<u>Instrumentation</u>. Two gas properties and five electrical parameters were measured to evaluate the performance of the generator.

Total pressure (P_o) was measured with a Bourdon tube pressure gage. Range: 0-300 psig. Probable error: $\pm$ 1 psi.

Total temperature (T_o) was measured with an iron-constantan thermocouple, type Y, and read directly from a Brown potentiometer recorder calibrated specifically for type Y iron-constantan. Range: -100 to +300 ^oF. Probable error: $\pm 2^o$.

The potential on the attractor (V_a) was read on a Sensitive Research Model ESH electrostatic voltmeter. Ranges: 0-5000, 0-10,000, 0-20,000, and 0-30,000 volts. Probable error: $\pm$ 0.5%.

The needle current (I_n) and the collector current (I_c) were measured on identical Weston Model 911 multiple-range ammeters. Ranges: 0-0.1, 0-0.3, 0-1.0, 0-3.0, 0-10, 0-30, 0-100 ma. Probable error: $\pm$ 1%.

The attractor current (I_a) was measured on one of three ammeters in series:

Ranges:	Probable errors:
0-30 μa	± 3%
0-100 μa	± 3%
0-500 μa	± 3%

When a ground plate was used, its current (I_{gp}) was also read on one of three ammeters in series:

Ranges:	Probable errors:
0-50 μa	± 3%
0-200 μa	± 3%
0-1.0 ma	± 3%

III. Theoretical Considerations

Although the work covered by this thesis was essentially experimental, some theoretical considerations were necessary or relevant. These included determination of the gas properties in the nozzles, understanding of corona discharge ionization, and estimation of the path of the ions in the nozzles. The specific numerical work done in this section was based on the geometry of Configuration VII, because it was the one selected for detailed analysis in this study and in Captain Wheeler's work (Ref 14).

Gas Flow in the Nozzles

Normally, isentropic flow would be assumed through convergent-divergent nozzles of the type used in the ionization region of the EHD generator, and calculations of gas properties would be based on the physical area ratios. However, due to the very small size of these nozzles, it was considered possible that the boundary layer might significantly alter the effective area ratios. Therefore, a rough analysis was made to determine the probable displacement thickness of the boundary layer, using the simplified relationships of Eckert and Drake (Ref 2:129-144). It was found that the worst conditions considered possible resulted in an effective exit area reduction of only 3%. Since this was not out of line with the general experimental accuracy, the boundary layer was neglected in computing gas properties in the nozzles.

Table II summarizes the necessary flow parameters in the nozzles for Configuration VII, based on three different total pressures and a typical total temperature of 0° F. Supersonic flow tables (Ref 1:21-22) were used.

Corona Discharge Ionization

The following brief discussion, in conjunction with Figure 11, presents the fundamentals of the corona discharge method of forming ions. This method was used in the EHD generator studied.

When a controlled potential difference is applied between the needle and attractor electrodes, a non-uniform electric field is created. The strong field in the vicinity of the needle point is able to ionize the air in that immediate region. (Technically, ionization occurs if the product of the mean free path and the electric field intensity exceeds the ionization potential of a molecule.) Farther from the point, however, the field is weaker, and an avalanche (complete breakdown) cannot occur.

This process can take place with either polarity of the applied field, and although there are significant microscopic differences between positive and negative corona mechanisms (Ref 13:6-10), the macroscopic effects during ion formation are the same. With the polarity shown in Figure 11, the negative ions remain at the needle (and release their extra electrons to the external circuit), while the positive ions are attracted outward into the gas stream. Their path is discussed on the following pages.

Ion Flow from the Corona

The movement of ions in a gas is governed by the concept of mobility, which is defined in the following quotation (Ref 13:2):

> When an ion in a gas is in the presence of an electric field, it is subject to the usual electrostatic force laws. In the resulting motion, it frequently collides with neighboring molecules. Therefore, it cannot accelerate indefinitely but quickly reaches an average velocity analogous to the terminal velocity of a particle falling through a viscous medium under the influence of gravity. This average velocity due to the electric field is given by the product of the mobility k of the gas, and the field strength E:
>
> $$u = kE \tag{1}$$
>
> where k has the defining equation:
>
> $$k = K\,\rho_o/\rho \quad (^*) \tag{2}$$
>
> where ρ is the density of air, and ρ_o (*) is the density of air at 0° C and 760-mm of Hg.

On the same page, the value of K in (m/sec) / (volt/m) is given as 1.6×10^{-4} for positive ions and 2.2×10^{-4} for negative ions, in pure dry air. If free electrons exist in the gas, their mobility is of the order of 10^4 greater than that of the ions (Ref 13:3), but they quickly attach themselves to a neutral molecule to form a negative ion.

---

*In this thesis, ρ_s is used instead of ρ_o for standard conditions.

The ions that are created in the nozzle by the corona are acted upon by the fluid flow and two electric fields. One field is that which is set up by the attractor potential, and the other is that due to the space charge of the ions themselves. Of course, the space charge field tends to shield the needle from the attractor, but to a rough approximation the effects can be studied independently.

<u>Effect of the Attractor</u>. An approximate determination of the effect of the attractor can be made by use of the following assumptions:

1. The field due to space charge is neglected.
2. The field due to the attractor is radial only, and exists only inside the cylindrical section defined by the attractor.
3. The grounded needle can be approximated by a grounded wire (of radius r_o) along the axis of the cylinder.
4. The gas velocity is axial only.
5. The gas velocity and density are constant over the length of the cylinder.
6. Induced magnetic fields are neglected.

These assumptions result in the following equation for the outside radius of a positive ion cloud as a function of the axial distance from the needle point (see Appendix C):

$$r_x^2 = r_i^2 - \frac{2\ k\ V_a}{v\ \ln\ (r_a\ /\ r_o)}\ x \qquad (3)$$

where
r_x = radius of ion cloud at station x (m)
r_i = assumed initial radius of ion cloud (m)
k = ion mobility (m^2/volt-sec)
V_a = attractor voltage (a negative value) (volts)
v = gas velocity (m/sec)
r_a = radius of attractor (m)
r_o = assumed radius of grounded wire along axis (assumption 3) (m)
x = axial distance from needle point (m)

Substitution of Eq (2) for the ion mobility k shows that, in addition to r_i, V_a/ρ is a controlling parameter.

$$r_x^2 = r_i^2 - \frac{2\,K\,\rho_s}{v\,\ln\,(r_a / r_o)}\,(V_a/\rho)\,x \qquad (4)$$

where K = a constant defined under Eq (2)
ρ_s = standard atmospheric density
ρ = actual gas density

Experimentally, it was determined that, for any ρ, V_a/ρ attained practically the same value just before sparkover. Therefore, Eq (4) can be plotted simply as r_x vs. x with r_i as a parameter. This is done, for Configuration VII, in Figure 12. A positive ion cloud was assumed, and r_a/r_o was taken to be 25. It can be seen that the field weakens rapidly away from the cylinder axis, and the ions should not reach the attractor before being swept downstream.

Effect of the Space Charge. Of major interest in predicting the path of the ions is the field due to the ion cloud itself, since this effect, while similar to that of the attractor in the region of the attractor, is present throughout the entire nozzle. The assumptions listed below lead to an approximation of the path of ion flow through the nozzle.

1. The gas velocity is axial only.
2. The gas velocity and density are constant over the length of the nozzle. (This assumption is discussed in detail in Appendix D.)
3. The charge density is constant over any one cross section.
4. The ion stream is nearly cylindrical; thus the electric field due to the space charge is radial only.
5. The field due to the attractor is neglected.
6. Induced magnetic fields are neglected.

Appendix D contains a derivation, based on the above assumptions, for the following equation, which is the profile of the ion cloud in the nozzle.

$$r_x^2 = r_i^2 + \frac{k\ I_n}{25\ e_o \pi v^2}\ x \qquad (5)$$

where	r_x	= radius of ion cloud at station x	(m)
	r_i	= assumed initial radius of ion cloud	(m)
	k	= ion mobility	(m^2/volt-sec)
	I_n	= total needle current	(amps)
	e_o	= permittivity of free space	(farad/m)
	v	= gas velocity	(m/sec)
	x	= axial distance from needle point	(m)

Again, substitution of Eq (2) for the ion mobility k shows the parameter of interest, this time I_n/ρ.

$$r_x^2 = r_i^2 + \frac{K\ \rho_s}{25\ e_o\ \pi\ v^2}\ (I_n/\rho)\ x \qquad (6)$$

Figure 13 is based on Eq (6), and shows the appearance of the expanding ion cloud as it flows down the nozzle. It is plotted for Configuration VII with a positive space charge, as was Figure 12. Upon consideration of the effect of the attractor, as presented in Eq (4) and Figure 12, the initial radius of the ion cloud at the needle point in Figure 13 was taken to be half the radius of the attractor; i.e., $r_i = r_a/2$. Profiles are shown for various values of I_n/ρ, with the line $I_n/\rho = 1.5 \times 10^{-3}$ amp/(lbm/ft^3) representing a typical high pressure run as accomplished experimentally.

It can again be noted that the field weakens as the radius of the cloud increases. This effect is pronounced at a small radius, of course, and tends to degrade the importance of the assumed value of r_1. This fact is illustrated by the single dashed curve plotted for $r_1 = 0$.

IV. Experimental Scope and Procedure

The experimental work for this thesis consisted of two separate phases. First was a determination of the current-producing capability of the EHD generator with each of the ten nozzle configurations shown in Figure 6. The second phase was additional investigation of the generator, under new conditions, using one particular nozzle configuration.

Evaluation of Nozzle Configurations

Scope. Complete current characteristics were determined for each of the ten nozzle configurations. Current characteristics are defined to be the curves of attractor current I_a, ground plate current I_{gp} (when a ground plate is used), and collector current I_c, plotted against the attractor voltage V_a. The parameters held constant for a given set of characteristics were total pressure P_0, total temperature T_0 (approximately), and transport region length L.

Characteristics were determined for three different total pressures: 100 psig, 150 psig, and 200 psig. These pressures were chosen for the following reasons: The lowest was high enough to assure full expansion in the nozzles; the highest approached the probable pressure limitation of the generator and the available capacity of the air supply; the third pressure was the midpoint between the high and the low.

The total temperature actually could not be controlled. Over the experimental period, it varied (depending on the outdoor ambient temperature) between extremes of -25° F and $+52^{\circ}$ F. However, as will be seen in the results, the variation of T_o in any one set of curves or experiments was much smaller than this.

Preliminary trial runs indicated that a transport region length of 0.5 inch was satisfactory. This was the middle of the range of available lengths, and was used for all current characteristics.

A negatively charged attractor was used for all runs in this series of tests. This had the effect of creating positive ions, which have a lower mobility than negative ions. At the time, this was thought to be desirable, since it would minimize the attractor and ground plate currents.

Procedure. The procedure for obtaining the current characteristics was as follows: First, the generator was assembled with the desired nozzle configuration. This involved selecting one of the two main nozzle types (attractor at exit plane, or attractor near the throat), and the proper number of spacers to correctly position the needle points. Next, the distance L was set at 0.5 inch, and flow was established with the first value of P_o. V_a was then raised in appropriate increments until sparkover occurred (if any), and V_a, I_a, I_{gp}, I_c, and T_o were recorded at each step.*

*Not mentioned here is the total needle current, I_n. It could not be measured at the time of these runs (but could later) because the needles were directly grounded through the generator support stand.

The raising of V_a and the recording of data were then repeated for the other two values of P_o.

Further Investigation of One Nozzle Configuration

After current characteristics had been found for all ten configurations, it was determined that the volt-ampere characteristics of the generator would be studied for Configuration VII. This study was accomplished by Captain H. P. Wheeler, and required extensive and careful insulation of the ion collector region (Ref 14:9). Following his work, further tests regarding ion flow were accomplished with Configuration VII.

Scope. Three additional investigations were made. They were as follows: the effect of density on the maximum currents obtained (P_o was varied from 80 psig to 240 psig); the effect of transport region length on the maximum currents obtained (L was varied from 1/8 inch to 1 inch); and a comparison of current characteristics for positive and negative ion flow.

Procedure. The effect of density was determined with L set at 0.5 inch, as before. With air flow established at one value of P_o, V_a was raised to a value close to sparkover voltage. The resulting values of I_a, I_{gp}, I_c, and I_n* were recorded, as well as T_o. This was then repeated for the other desired values of P_o.

The effect of the length of the transport region was studied at both 150 psig and 200 psig. For a certain length L, and for the two

*By this time, an insulator had been built into the generator support stand, allowing direct measurement of the total needle current.

pressures in turn, V_a was raised to just below sparkover voltage. T_0 and the resulting values of I_a, I_{gp}, I_c, and I_n were recorded. The generator was then shut down, the collector reset to provide a new L, and the above procedure repeated.

For a comparison of positive and negative ion flow, the procedure already described for obtaining current characteristics was again followed. It was necessary first to run new characteristics for positive ion flow to avoid the effects of a large difference in T_0. Then the Beta power supply was rewired to furnish a positive potential V_a, yielding a negative ion flow through the generator. For these runs, the polarity of all ammeters had to be reversed.

V. Results and Discussion

This chapter presents and discusses the results of the experimental work, primarily by graphical means (Figures 14 through 26). All the original data for the curves, and some data which is not plotted, is tabulated in Appendix E.

Evaluation of Nozzle Configurations

Configurations I, II, and III. Complete current characteristics for Configurations I, II, and III are shown in Figures 14, 15, and 16 for the three different total pressures used (100, 150, and 200 psig). At any one pressure, the only significant difference among the configurations was the magnitude of attractor voltage required to obtain a given current. With increased pressure, all maximum collector currents increased, and relative to them, the attractor currents decreased. Also, the peak collector currents occurred at higher attractor voltages.

The attractor potential was not raised to the sparkover voltage for these configurations, because as V_a was increased, I_c tended to reach or approach a maximum value while I_a increased very rapidly.

Since I_a represents the electrical input, its high value and steep slope indicate that a generator using this type of nozzle design would have a large input power which would also be very sensitive to a change in attractor potential.

It is probable that the performance would have been improved by a needle point position farther forward than any of those used, but the location in Configuration I was the limit of the available geometry.

Configurations IV - X. Because of the large attractor current indicated above, and because of the desirability of a ground plate for the mechanism of power production (Ref 14:7), the type of nozzle represented by Configurations IV - X was adopted.

It was found that IV and V, where the needles were far forward, were completely unsatisfactory: sparkover from the attractor to the needle shaft occurred before any (IV) or almost any (V) current was produced. The other configurations all yielded significant currents, and their current characteristics (except for X) are presented in Figures 17, 18, and 19 for the same total pressures as for I - III. Configuration X was omitted for the sake of clarity; it continued the downward performance trend of IX.

For each characteristic shown (except that of IX at 100 psig, for which no sparking was visible), V_a was raised until field breakdown occurred. This was at progressively higher voltages for the higher pressures, which was expected from the normal breakdown voltage vs. pressure relationship, or Paschen curve (Ref 6:54). The location of the sparkover varied: It was from the attractor to the needle in VI and the two lower pressures of VII, while in the high pressure of VII and in VIII and IX it was from the attractor to the ground plate.

The outstanding result shown by this group of current characteristics was the high collector current (potential power output) which could be obtained with a very small attractor current (power input) by the proper combination of pressure, nozzle configuration, and attractor voltage. Also, the ground plate current, which was a loss of ions successfully produced by the needles, could be held to a reasonably low value.

Figure 20, a cross-plotting of the current characteristic data, summarizes most of the above information. The maximum collector current obtained is plotted against the nozzle configuration, with pressure as a parameter. The factor that limited the current is indicated: field breakdown from attractor to needle, field breakdown from attractor to ground plate, or a peaking of current before a breakdown occurred. Also shown are two arbitrary practical limitations where I_a became a certain percentage of the value of I_c. It easily can be seen that the optimum configuration for P_o = 100 psig and P_o = 150 psig lay somewhere between VII and VIII. Similarly, a design between VI and VII was probably most favorable for P_o = 200 psig. Therefore, of the actual configurations available, VII was considered to be the most favorable overall, and was selected for further study. This was an interesting contrast with the results reported by Petruzzella: his most closely comparable geometry obtained the highest current when the needle protruded slightly through the attractor (Ref 7:4).

Further Investigation of Configuration VII

Effect of Density. Figure 21 shows the effect of the air density (or total pressure) on the maximum currents created in the generator. Plotted against P_o are I_n, I_c, I_{gp}, and I_a, as well as a previously undefined current, I_{esc}. I_{esc} is the current which escaped through the collector due to incomplete neutralization of the ion stream. Its relative magnitude is known to depend largely on the effective length-to-diameter ratio of the collector passages, because of the mutual repulsion of the flowing ions. The escaping current could not be measured directly, but since I_n was the total current through the needles, I_{esc} could be computed from

$$I_{esc} = I_n - (I_c + I_{gp} + I_a) \tag{7}$$

For the collector used, I_{esc} was found to be about 15% of I_c in the higher current ranges.

The behavior of the needle current was worth noting. Up to a total pressure of approximately 160 psig, I_n increased rapidly with density, and was limited in each run by breakdown from the attractor to the needles. Beyond P_o = 160 psig, I_n was limited by breakdown from the attractor to the ground plate. In this regime, the rate of increase of I_n decreased, and it appeared that a pressure could be reached beyond which I_n would remain constant.

The I_n vs ρ relationship was reflected in the ground plate current, which built up to a maximum value at 160 psig total pressure and then decreased. It can be recalled from Eq (6) that the spreading of the ion stream in the nozzle depends on the ratio I_n/ρ. Thus I_n/ρ_o should have increased at first, attained a maximum value at P_o = 160 psig, and decreased thereafter. Table III indicates that this was indeed true.

Effect of Length of Transport Region. The same maximum currents as above, I_n, I_c, I_{gp}, I_{esc}, and I_a (negligible), are plotted against L in Figures 22 and 23 for P_o = 150 psig and P_o = 200 psig respectively. The data was more scattered than in previous investigations, but the trends discussed below were readily apparent.

The production of total current (I_n) was unaffected by the length of the transport region. This desirable characteristic indicated that the ground plate did in fact serve as an effective shield between the ionization region and the electric field of the transport region.

An increase of L, especially at longer distances, caused a considerable shift of current from the collector to the ground plate. This was probably due to the following effects: The axial electric field in the transport region, caused by the space charge, increased with length. This retarded the ion flow more strongly. At the same time, the ion stream had a longer period in which to expand laterally under the influence of the radial field. This allowed more ions to find their way into the boundary layer and other comparatively stagnant regions of gas flow, in which they migrated back to the ground plate.

The escaping current remained constant as L increased, even though I_c decreased. This indicated that the larger the current was through the ion collector, the greater was the neutralization efficiency.

The ratio I_{esc} / I_c varied from 0.13 to 0.25 over the range involved in Figure 22, and from 0.10 to 0.20 in Figure 23.

Comparison of Positive and Negative Ion Flows. The current characteristics for Configuration VII for both positive and negative ion flows are presented in Figures 24, 25, and 26. (Except for a higher T_o, the curves for positive ions are the same as for VII in Figures 17, 18, and 19.)

The most apparent contrast was the significantly higher currents that were obtained with negative ions. This was also reported by Petruzzella (Ref 7:5), and was because the greater mobility of negative ions allowed a more rapid expansion of the original clouds of charge at the needle points. The greater mobility of negative ions was also reflected by the much higher percentage of negative current which reached the ground plate.

The attractor voltage for field breakdown (sparkover to the needle) appeared to depend on the ion polarity to some degree. At P_o = 100 psig, the breakdown voltages for positive and negative ion flows were about the same. At P_o = 150 psig, breakdown occurred at a higher V_a for negative ions, and the difference was even larger at P_o = 200 psig.

These comparisons are summarized in Table IV.

Other General Discussion

It is interesting to compare the experimental values of I_n / ρ to Figure 13, which shows profiles of ion stream expansion in the nozzle. From Table III, the maximum value of I_n / ρ_o obtained experimentally was 640 $\mu a/(lbm/ft^3)$. This corresponds to $I_n/\rho_{avg(2-3)} = 1.7 \times 10^{-3}$ amp/(lbm/ft^3), which lies just above curve 3 on Figure 13. It can be seen that the profiles give only a qualitative indication of the true path of the ions, since a significant ground plate current actually existed at this current-density ratio.

General Electric Company has stated that the major limitation of the corona discharge technique of ionization is the limited current (about 10 μa) which a corona point can produce (Ref 9:76). However, Petruzzella achieved a maximum current of 160 μa from a single needle (Ref 7:42). His diameter of flow at the needle point was double that used by General Electric. On the other hand, the flow diameter at a needle point of the generator tested for this thesis was only half of the diameter used by General Electric, and with Configuration VII, at P_o = 200 psig, each needle produced roughly 28 μa. At the highest pressure used (P_o = 240 psig), the current per needle was 30 μa. (Data taken from Figure 21, divided by the number of needles, 25.) This certainly shows that geometry and gas flow properties have a great influence on the output of a corona discharge needle.

Of greater interest and validity than absolute current output is the average ion concentration, N, that is furnished by the ionization region of a generator. This can be determined (with a change of units) from Eq (D-9) of Appendix D by using the radius of the nozzle exit instead of the radius of the ion stream. The ion concentration is directly proportional to the needle current, and for Configuration VII is given numerically by

$$N = 5.06 \times 10^{13} \times I_n \quad \text{ions/cm}^3 \qquad (8)$$

where I_n is the total needle current in amperes. Again from Figure 21, $I_n = 710 \times 10^{-6}$ amperes for $P_o = 200$ psig. This yields an ion concentration of 3.6×10^{10} ions/cm^3. For comparison, Gourdine's initial experiment (Ref 4:5) produced an estimated 10^6 ions/cm^3, General Electric obtained approximately 5×10^9 ions/cm^3 (Ref 9:78), and Petruzzella's data (Ref 7:11,42) indicated a maximum of about 2×10^{10} ions/cm^3.

Successful production of ions must be accompanied by a satisfactory flow pattern. That is, flow to the attractor must be minimized while flow to the collector is maximized. All configurations of the type using a ground plate could be operated successfully in this regard as can be seen in Figures 17-19, and as is shown more explicitly in Figure 20 by the $I_a = 5\% \ I_c$ and $I_a = 10\% \ I_c$ lines. In fact, for Configuration VII (using accurate I_a data from Appendix E), it was found that at the three nominal total pressures of 100, 150, and 200 psig, I_a was in the range of 1.1% to 1.4% of I_c at the maximum level of current production.

Although investigation of power characteristics was outside the scope of this study (Wheeler covers it thoroughly, Ref 14), it is certainly worth noting that the ion flow patterns discussed above were very favorable for net electrical power production. For example, at P_o = 200 psig, the electrical input power to Configuration VII (through the attractor, given by $V_a I_a$) was about 0.09 watt. At the same time, the output power delivered to an appropriate load resistor was approximately 9.0 watts. In other words, an electrical power feedback of 1.0% of the output would have been sufficient for self-excitation of the generator. The unquestionably large aerodynamic losses in the gas flow were not investigated by this author or by Wheeler.

VI. Conclusions

The following conclusions can be drawn from this study of ion production and flow in an EHD generator. The first three are general in nature. The remainder apply specifically to the generator investigated, but should be valid and useful for any similar type of machine.

1. Direct conversion of fluid flow energy to electrical power through the use of an electrohydrodynamic generator is possible.

2. Corona discharge is a practical method of ionization. A proper configuration of electrodes can hold the attractor current, or electrical power input, to an essentially negligible value.

3. The concept of multiple corona discharge needles, located in a group of parallel nozzles, is good. Compared to a single needle, multiple needles provide more nearly one-dimensional electric and fluid flow fields in the transport region, and also furnish a larger current for investigation.

4. All the basic requirements of the EHD energy conversion process were fulfilled very well by the generator tested.

5. It was desirable to have the attractor plate located some distance upstream from the nozzle exit plane, as in Configurations IV - X. This removed it from the effects of turbulence and boundary layer in the transport region, and allowed only a minimum attractor current.

6. Particularly in the higher pressure ranges, Configuration VII (in which the needle points were located at the axial midpoint of the attractor plate) was the most favorable of all those tested. However, Figure 20 shows that it was not the optimum at any of the specific pressures used. At P_o = 100 psig and 150 psig, a more upstream needle position was best, and at P_o = 200 psig, the optimum needle position appeared to be somewhat downstream from that of VII.

7. The density of the flowing gas was of prime importance in the performance of the generator. Figure 21 shows that the collector current increased greatly with increasing gas density.

8. The length of the transport region did not affect the production of ions in the ionization nozzles, but did affect the resulting ion flow. Figures 22 and 23 indicate this. The ground plate apparently served as an effective shield between the ionization and transport regions.

9. Figures 24 through 26 show that the generator operated with potential of either polarity applied to the attractor. The resulting ion production, however, was higher for a positive attractor; that is, when the ions carried through the generator were negative.

VII. Recommendations

It appears certain that more work should be done in regard to electrohydrodynamic energy conversion. Many broad areas for further investigation and study are well outlined by Lawson (Ref 6:13-23), and will not be repeated here. However, findings from this study seem to warrant several recommendations relative to the design and further testing of the specific type of generator used in this work. They are as follows:

1. Since the needle point location was most favorable in the region limited by Configurations VI and VIII, it would be desirable to investigate the effect of several additional positions within that region. This could be done easily by obtaining one or more new, thinner, needle position spacers of the type shown in Figure 6, and would furnish more accurate information regarding the current maximums shown in Figure 20.

2. The breakdowns which occurred between the attractor and the needle shaft in the more forward needle positions might be avoided if a method were devised to insulate the body of the needle, leaving only the tip exposed.

3. To help avoid concentration of electric field lines, and the resultant early sparkover, all exposed edges of the attractor and ground plate should be well rounded. Also, the holes through the ground plate should continue the divergence of the nozzle

in order to minimize further the ground plate current.

4. The ion collector could be lengthened to reduce the number of ions that escape without being neutralized, or a variable-length collector could be built to study the actual relation between collector length and the escaping current. Also, the present collector could be tested without the screen on the upstream end (it is a serious flow restriction) to determine its relative effectiveness.

5. If it were determined that the present generator could safely take a higher total pressure, tests should be made with P_o in the range of 300 to 400 psig. This would indicate the higher pressure trends that can only be inferred from Figure 21. It would be well to design any new generator for such pressures.

6. The generator has a demonstrated capability of operating with a potential of either polarity on the attractor. A logical and important next step would be to apply an alternating potential in order to study the alternating current possibilities of the EHD generation process.

7. The aerodynamic losses should be studied. In this generator, they are undoubtedly large, as it was designed primarily according to electrical criteria. Further designs should incorporate great aerodynamic improvements.

8. One final suggestion, further removed from the presently available equipment, is to use a liquid for the working fluid. Stuetzer (Ref 11) has done considerable work along this line. He

has produced, by the corona discharge method, an ion concentration of 6×10^{11} ions/cm^3 (a factor of 10 greater than the value reported in this work) in kerosene, whose ion mobility is 2×10^{-7} m^2/volt-sec (1000 times less than that of air at standard conditions) (Ref 11:19, 21).

Bibliography

1. Ames Research Staff. Equations, Tables, and Charts for Compressible Flow. NACA Report 1135. Washington: National Advisory Committee for Aeronautics, 1953.

2. Eckert, E. R. G., and R. M. Drake, Jr. Heat and Mass Transfer. New York: McGraw-Hill Book Co., 1959.

3. Gourdine, M. C. Power Addition and Extraction from Gas Flow by Means of Electric Wind. Jet Propulsion Laboratory Technical Report 32-18. Pasadena, California: California Institute of Technology, 1960.

4. -----. Power Generation by Means of the "Electric Wind". Jet Propulsion Laboratory Technical Report 32-6. Pasadena, California: California Institute of Technology, 1960.

5. Harris, D. J. The Direct Generation of Electric Power from a High Velocity Gas Jet. Conference Paper 61-1091. New York: American Institute of Electrical Engineers, 1961.

6. Lawson, M., H. Von Ohain, and F. Wattendorf. Performance Potentialities of Direct Energy Conversion Processes Between Electrostatic and Fluid Dynamic Energy. Aeronautical Research Laboratory Technical Report 178. Dayton, Ohio: Wright-Patterson Air Force Base, 1961.

7. Petruzzella, N. L. Corona Discharge-Aerodynamic Ion Flow Study. Unpublished independent study. Yellow Springs, Ohio: Antioch College, 1959.

8. Robinson, M. "Movement of Air in the Electric Wind of the Corona Discharge." Communication and Electronics, 54:143-150 (May 1961).

9. Sherman, A., J. M. Smith, et al. Study of Electrical Energy Conversion Systems. Aeronautical Systems Division Technical Report ASD-TR-61-704. Dayton, Ohio: Wright-Patterson Air Force Base, 1962.

10. Smith, J. M. Theoretical Study of the Electrohydrodynamic Generator. General Electric Technical Report R 61 SD 192. King of Prussia, Pennsylvania: General Electric Company Space Sciences Laboratory, 1961.

11. Stuetzer, O. M. "Ion Transport High Voltage Generators." *The Review of Scientific Instruments*, *32*:16-22 (January 1961).

12. Velkoff, H. R. *Electrofluidmechanics: A Study of Electrokinetic Actions in Fluids*. Project 3141, Aeronautical Systems Division Propulsion Laboratory. Dayton, Ohio: Wright-Patterson Air Force Base, 1961.

13. Werner, F. D., and R. L. Geronime. *Investigation of a Corona Discharge for Measurements in Air Flow*. Rosemount Aeronautical Laboratories Research Report 84. Minneapolis, Minnesota: University of Minnesota, 1952.

14. Wheeler, H. P., Jr. *The Volt-Ampere Characteristics of an Electrohydrodynamic Generator*. Unpublished thesis. Wright-Patterson Air Force Base, Ohio: Institute of Technology, 1962.

Appendix A

Figures and Tables I, II, III, and IV

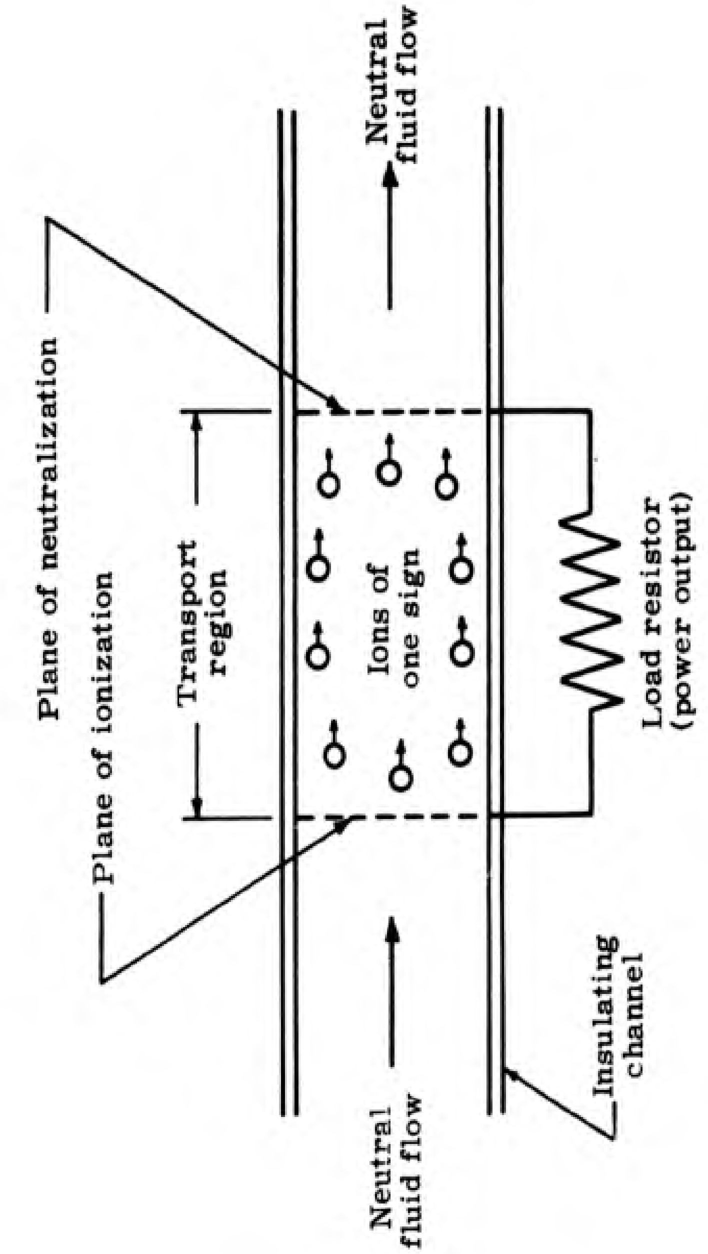

FIGURE 1

The EHD Power Generation Process

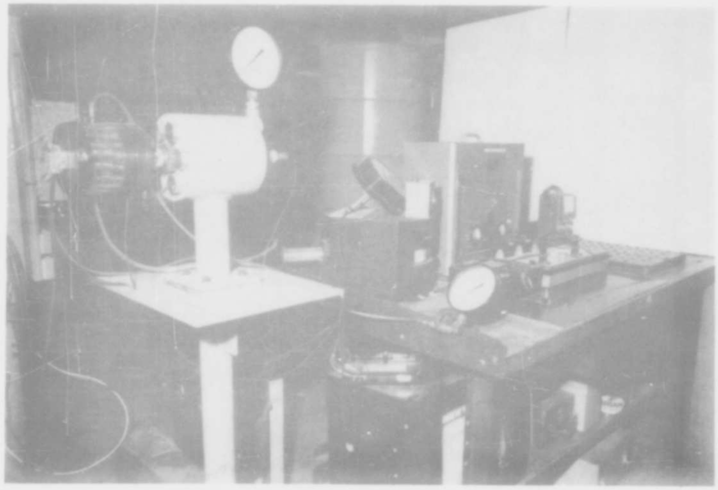

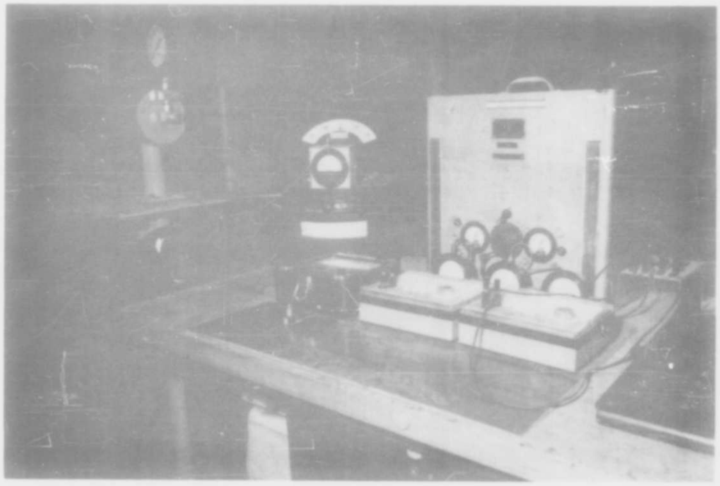

FIGURE 2

Experimental Apparatus

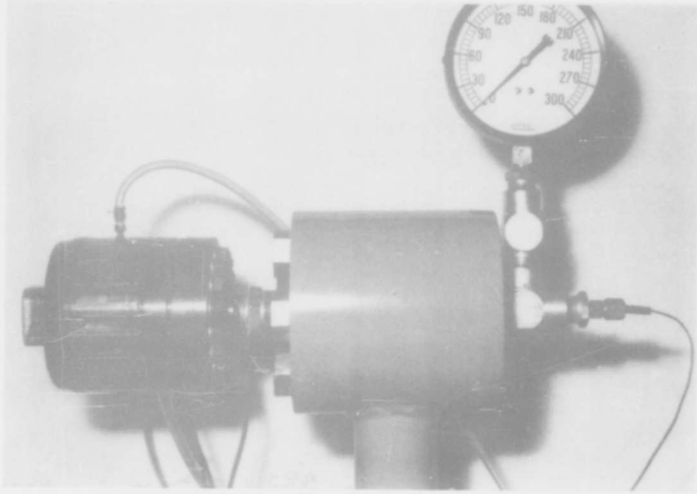

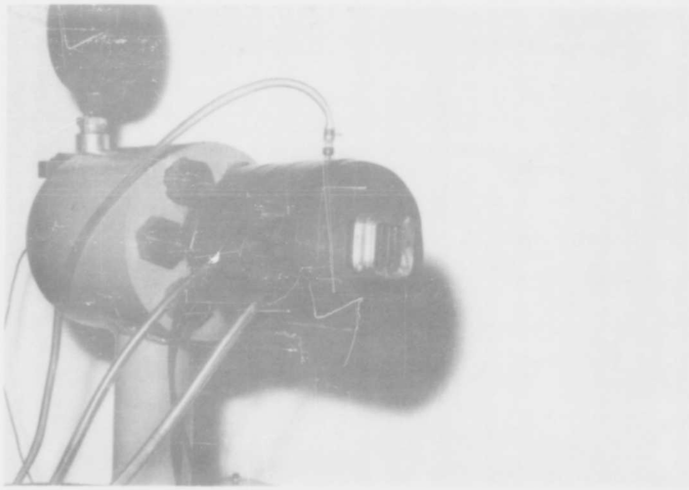

FIGURE 3

The Electrohydrodynamic Generator

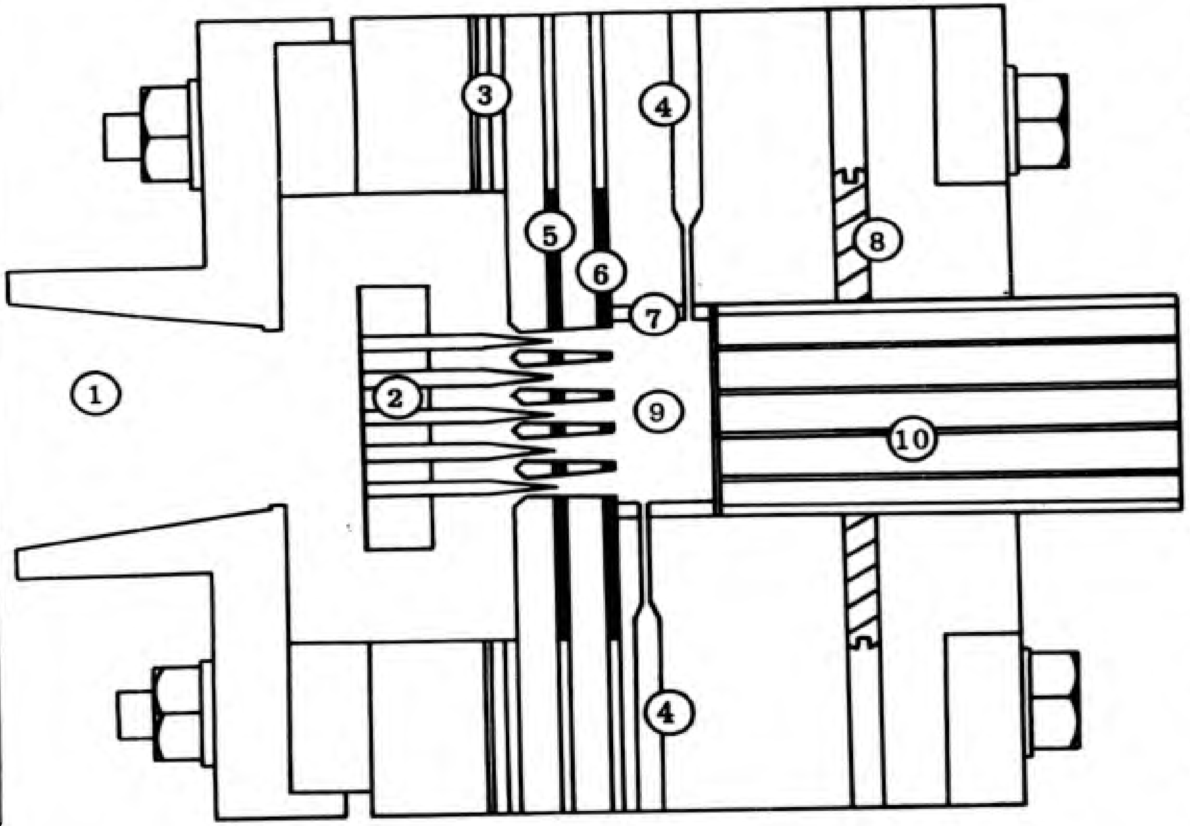

1. Entrance from reservoir
2. Corona discharge needles
3. Spacers to establish needle position
4. Static pressure tap (not used in this study)
5. Attractor plate (in mid-nozzle position)
6. Ground plate
7. Spacers to establish length of transport region
8. Setscrew to hold collector in position
9. Transport region
10. Ion collector

FIGURE 4

Full Size Sectional Side View of the EHD Generator

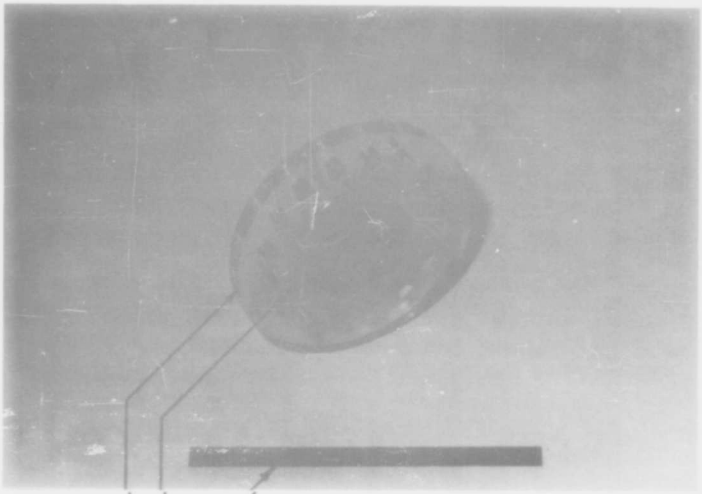

6-inch scale
Attractor plate
Plastic disk containing nozzles

FIGURE 5

Attractor Plate, Mounted at the Nozzle Exit Plane

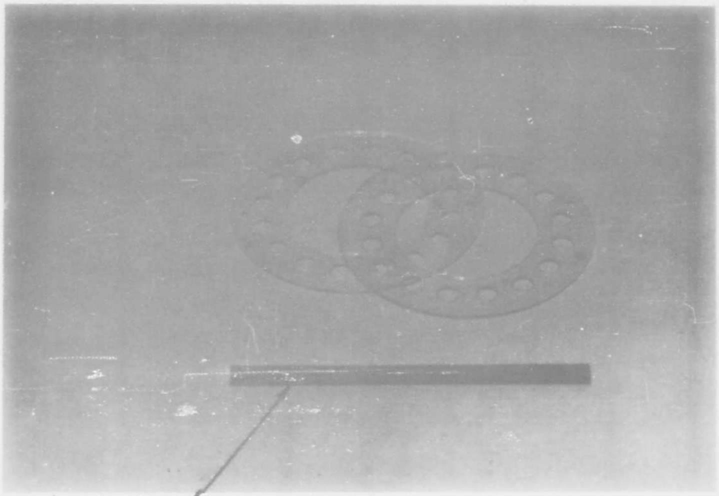

FIGURE 6

Needle Position Spacers

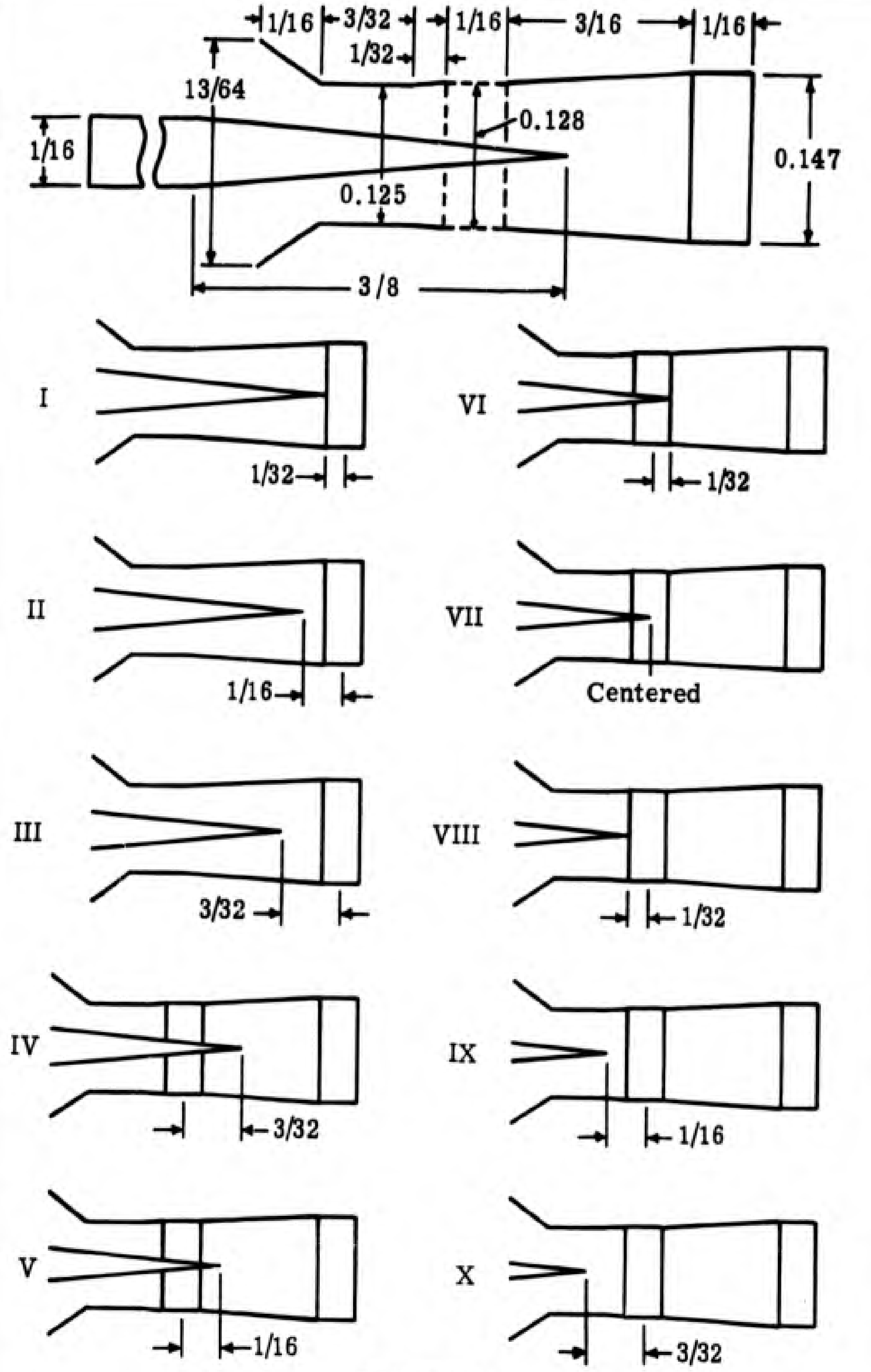

FIGURE 7

Nozzle Configurations Investigated

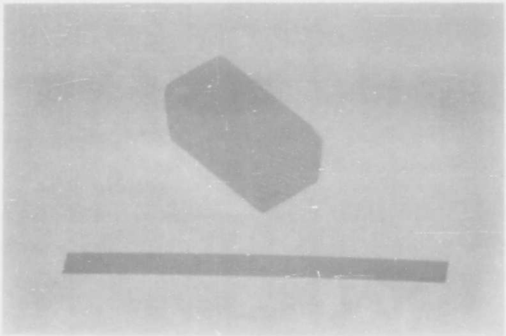

Upstream end

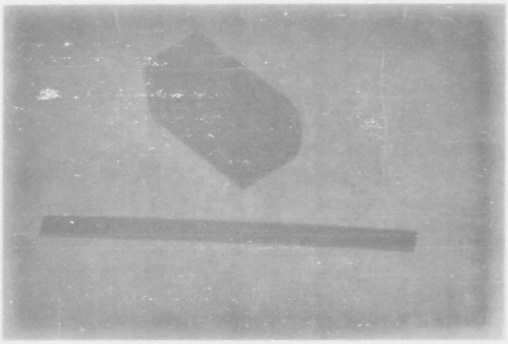

Downstream end

FIGURE 8

Ion Collector

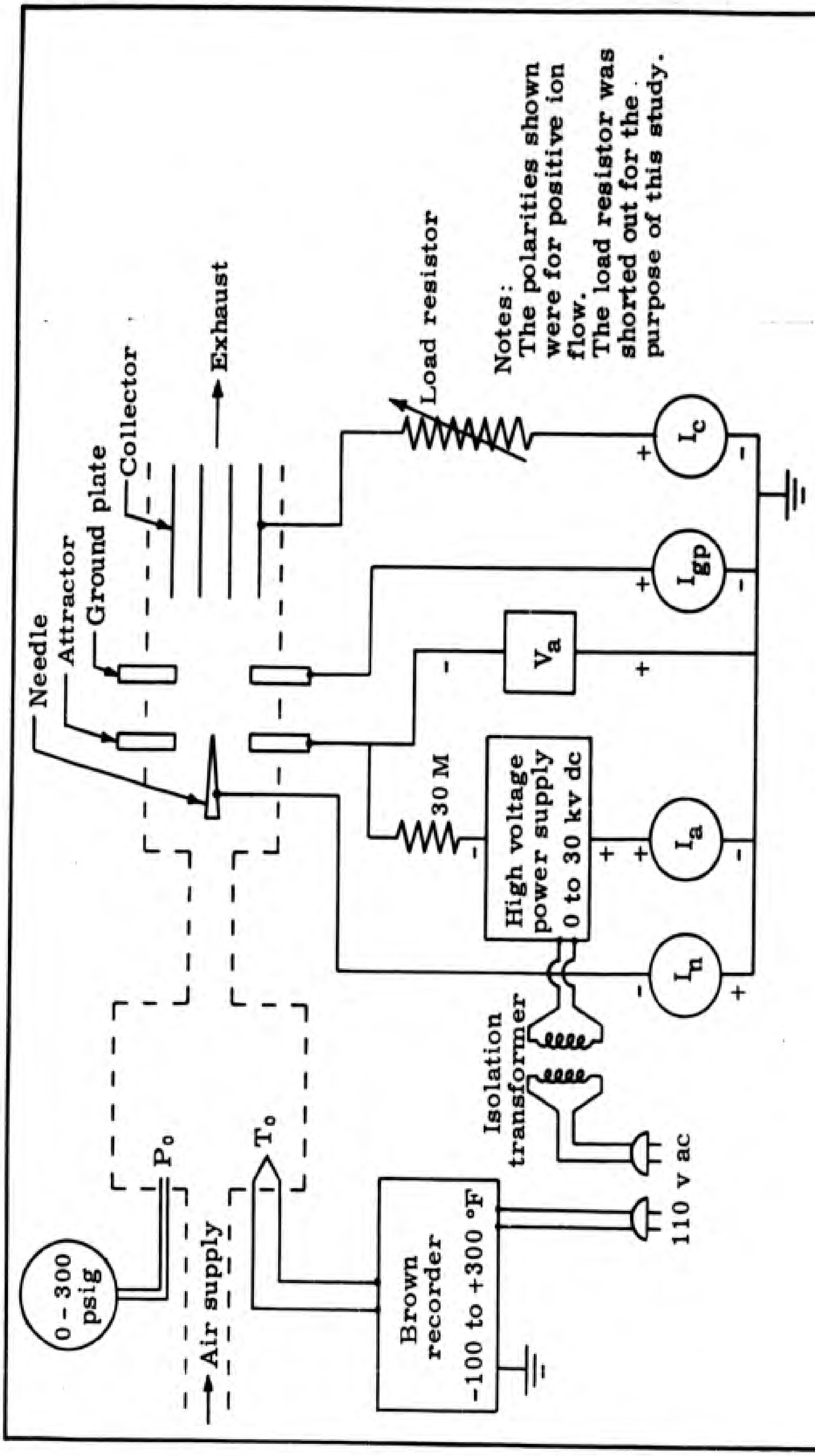

FIGURE 9

Schematic Diagram of the Apparatus

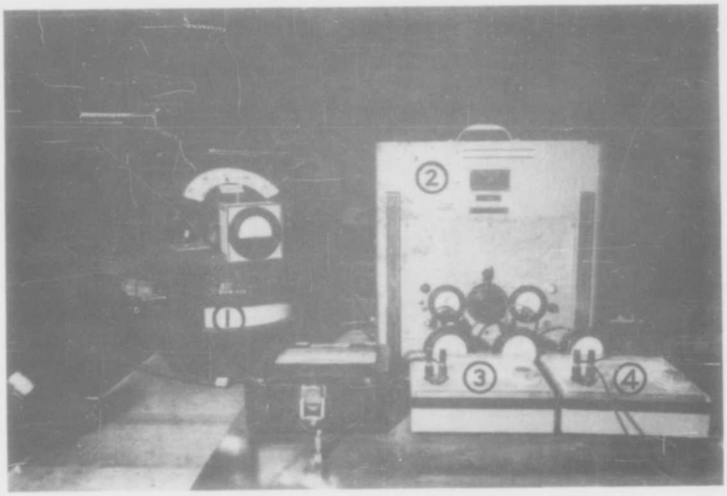

(1) Voltmeter for attractor potential

(2) High voltage power supply

(3) Ammeter for needle current

(4) Ammeter for collector current

Three ammeters for ground plate current are behind (3) and (4)

Three ammeters for attractor current are near (1)

FIGURE 10

Power Supply and Electrical Instrumentation

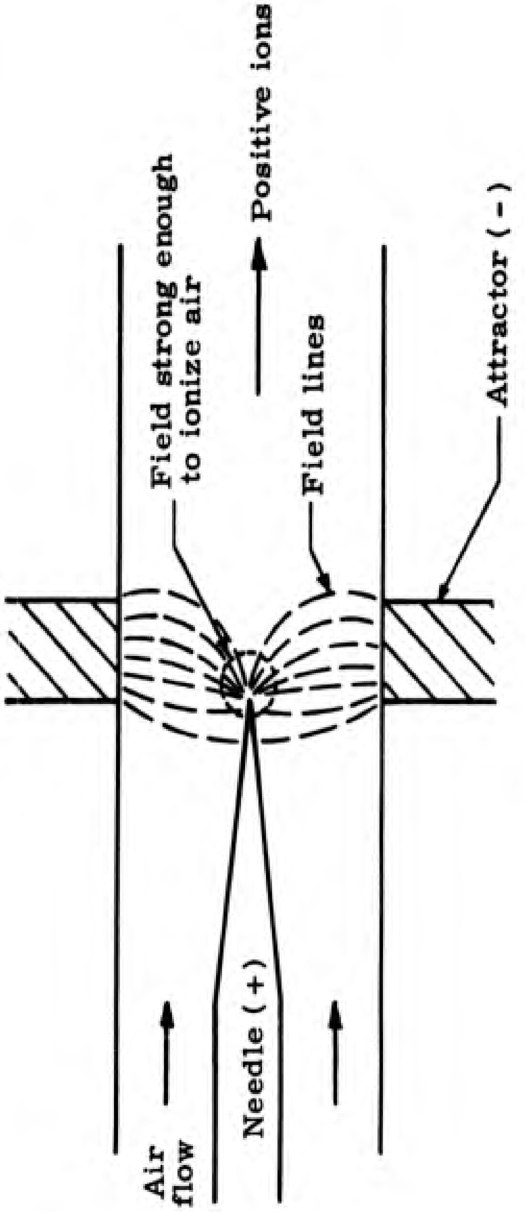

FIGURE 11

Corona Discharge Ionization

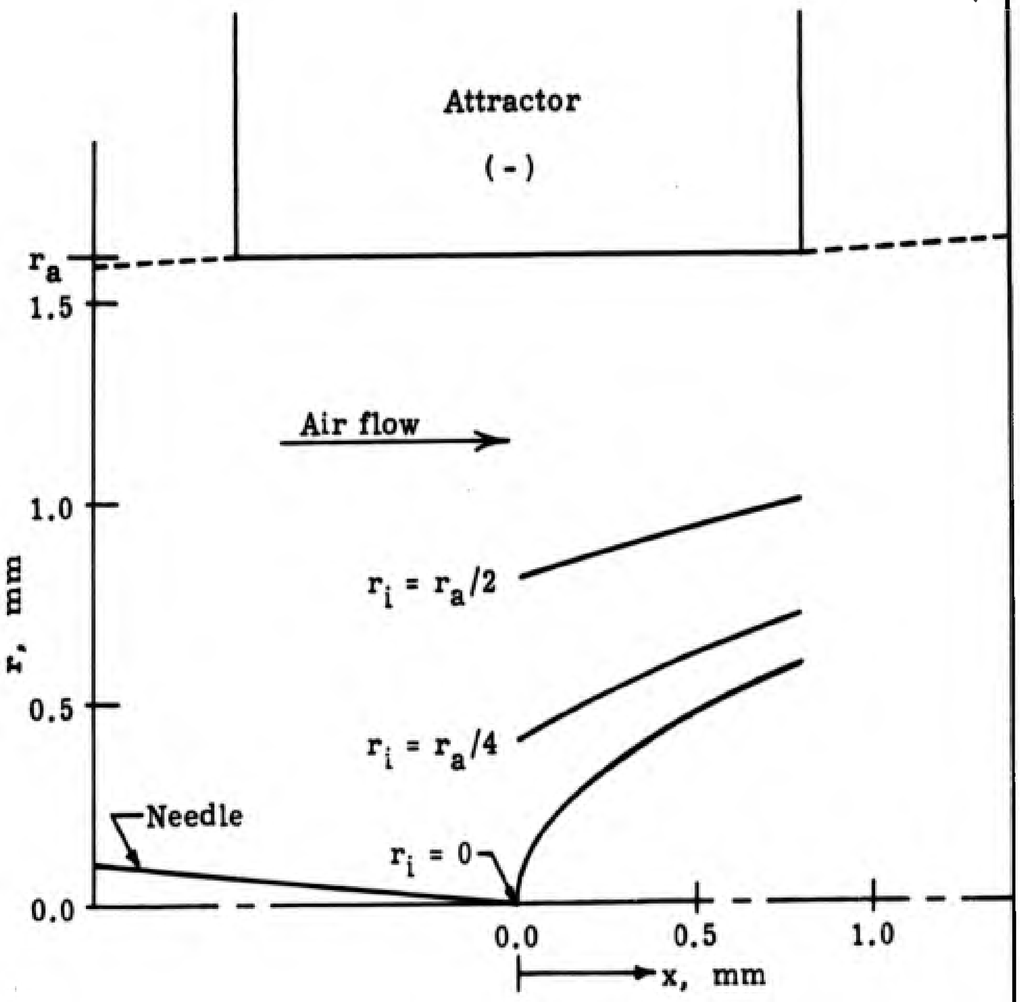

Notes:
Paths shown are for positive ions.
Attractor is just below sparkover voltage.
The field due to space charge is neglected.

FIGURE 12

Profile of Ion Cloud Expansion Due to Attractor
(Configuration VII)

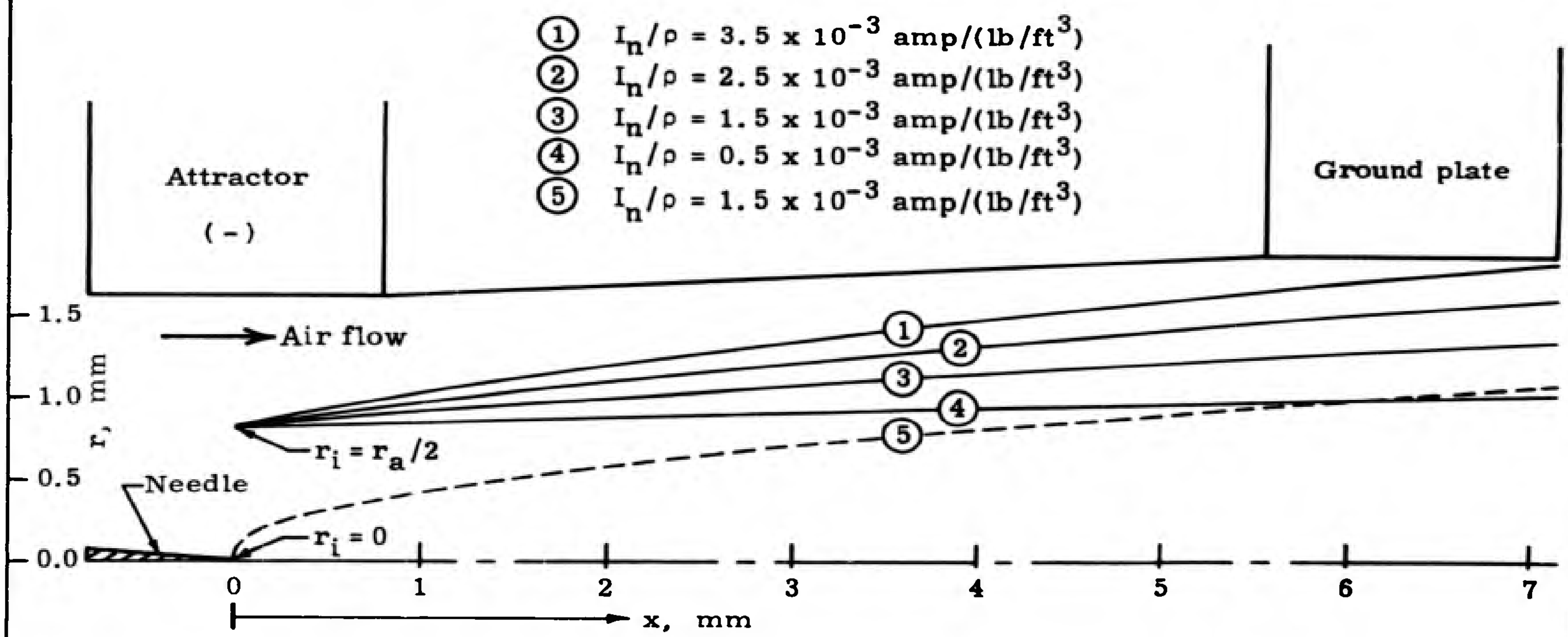

Notes:
Profiles shown are for positive ions.
The field due to the attractor is neglected.

FIGURE 13

Profile of Ion Stream Expansion in Nozzle
(Configuration VII)

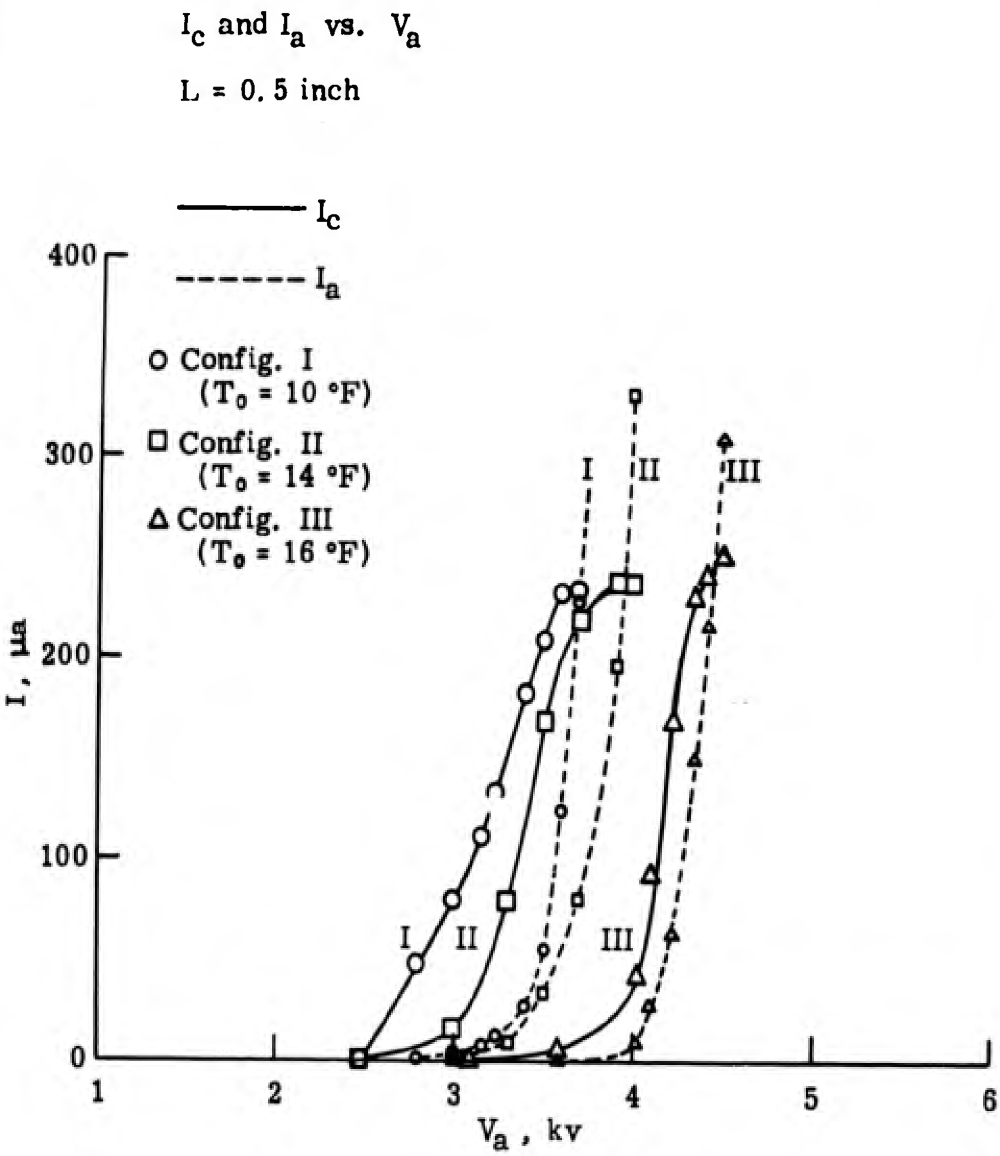

FIGURE 14

Current Characteristics for Configurations I, II, and III (P_0 = 100 psig)

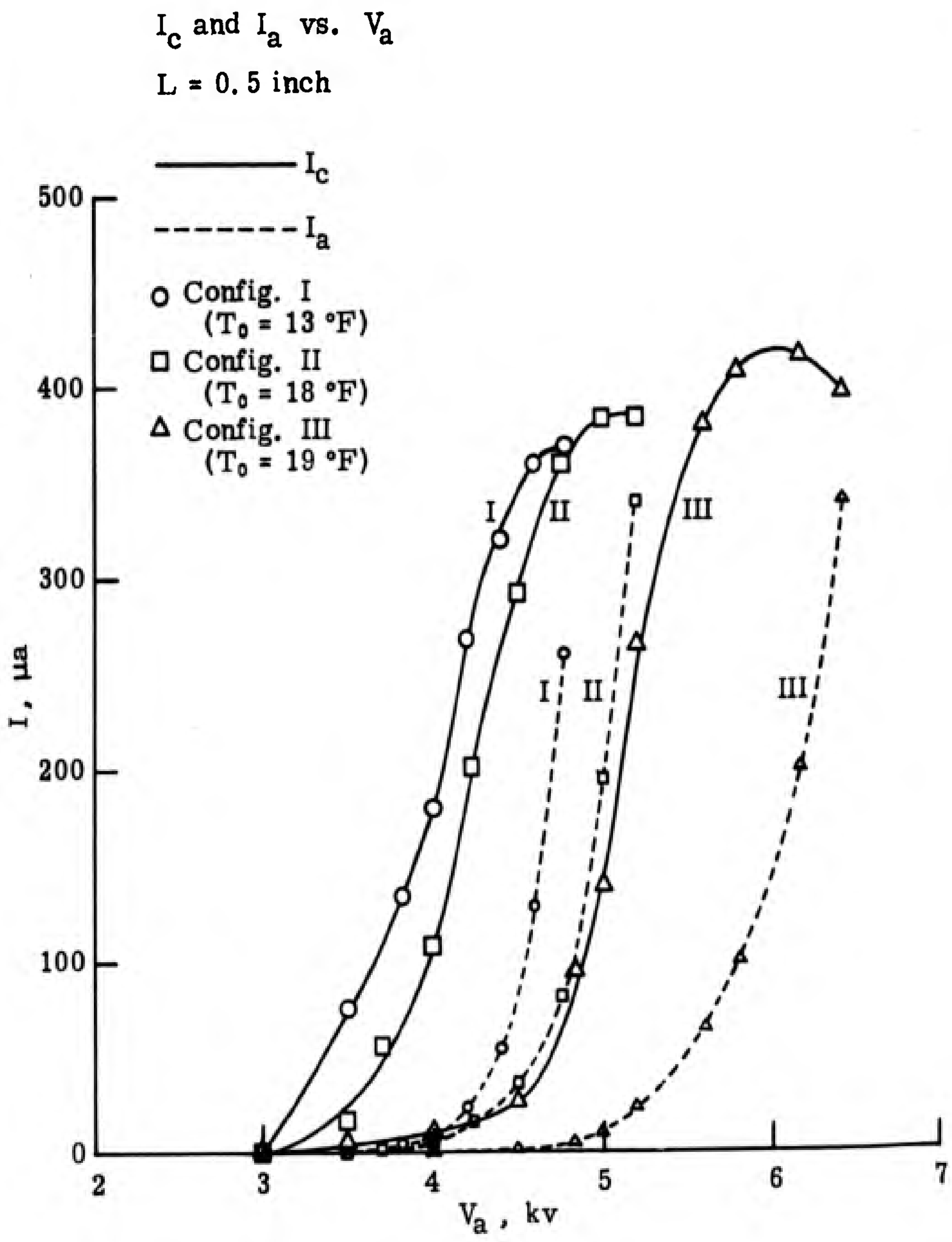

FIGURE 15

Current Characteristics for Configurations I, II, and III
(P_0 = 150 psig)

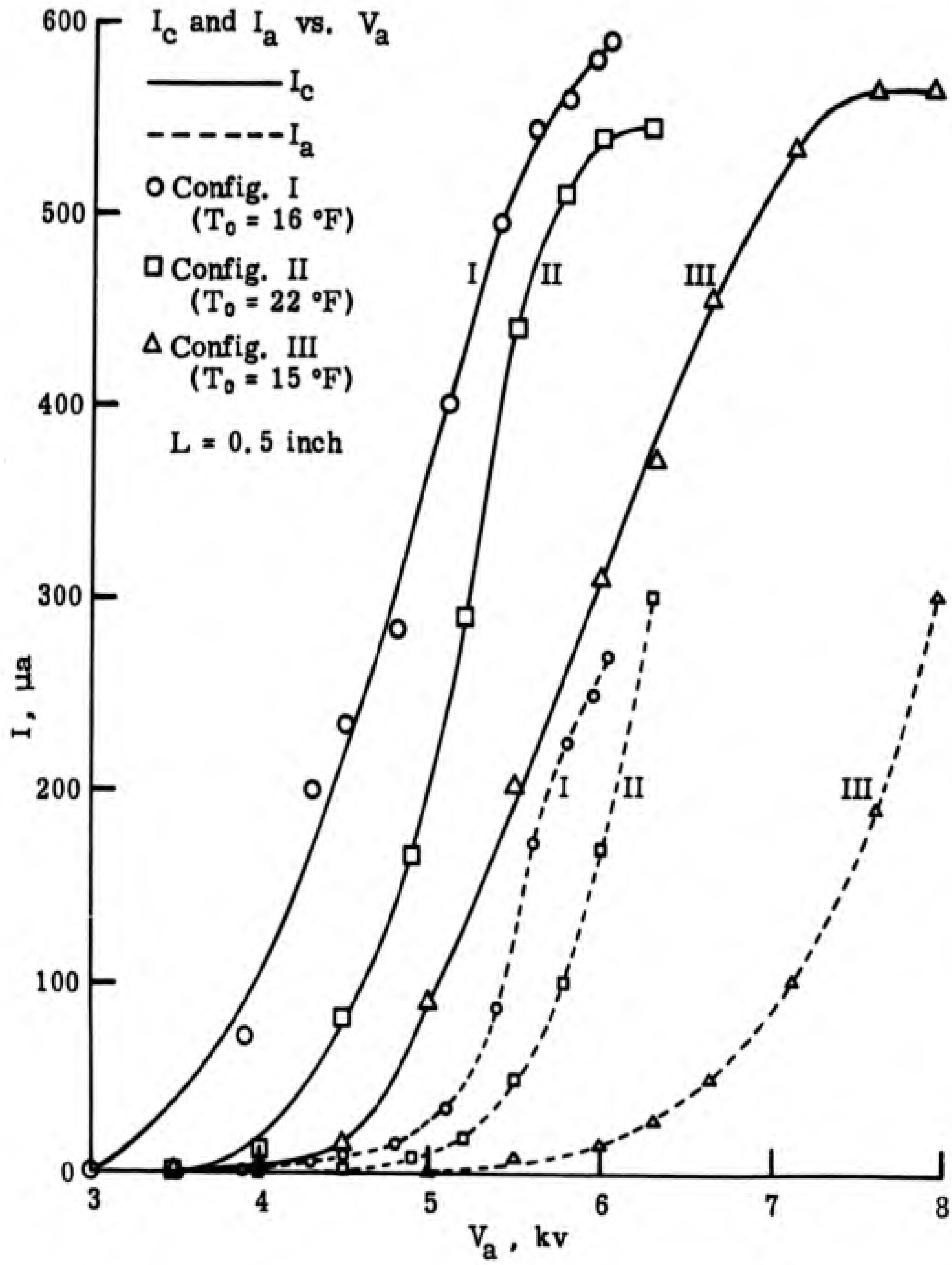

FIGURE 16

Current Characteristics for Configurations I, II, and III
(P_0 = 200 psig)

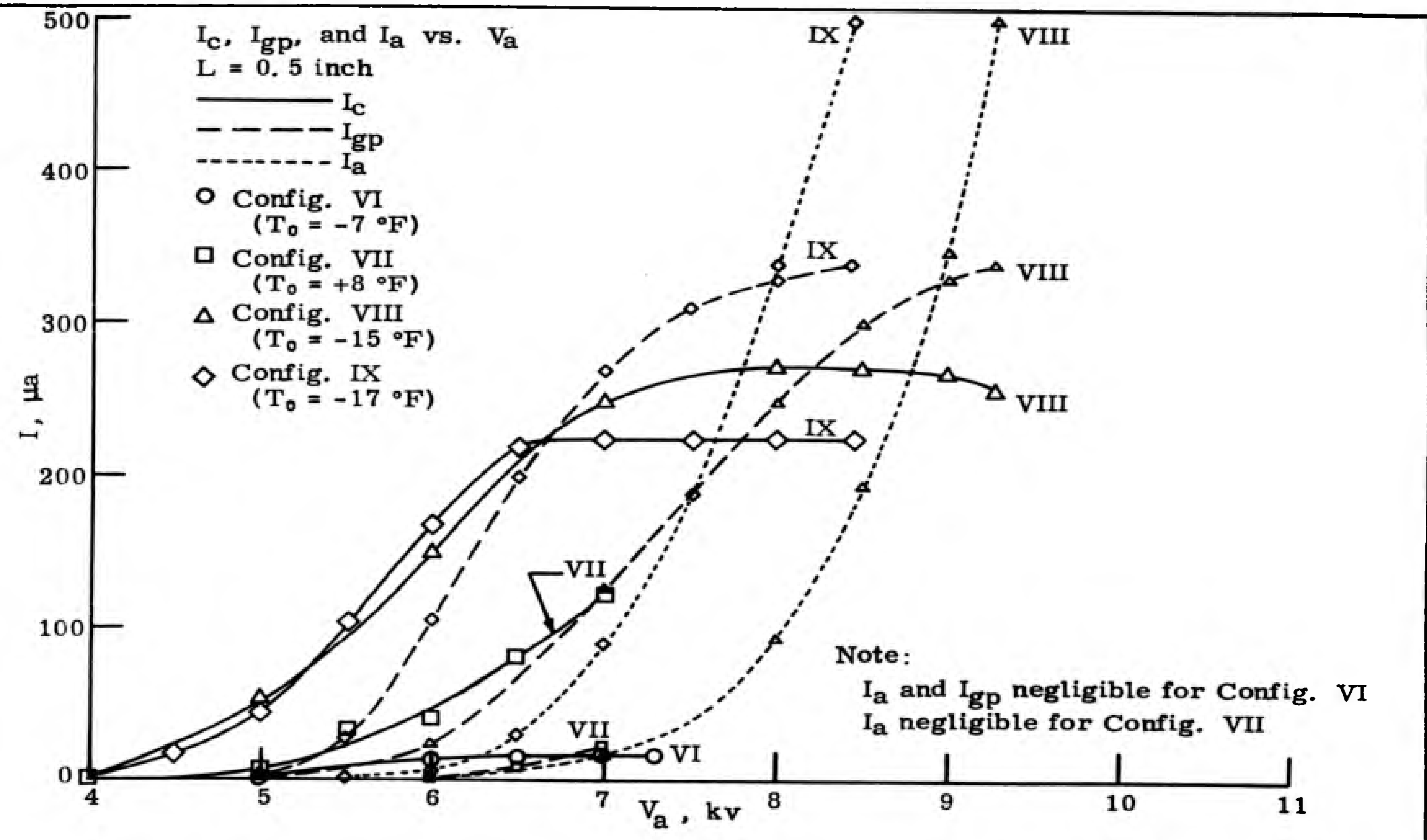

FIGURE 17

Current Characteristics for Configurations VI, VII, VIII, and IX (P_0 = 100 psig)

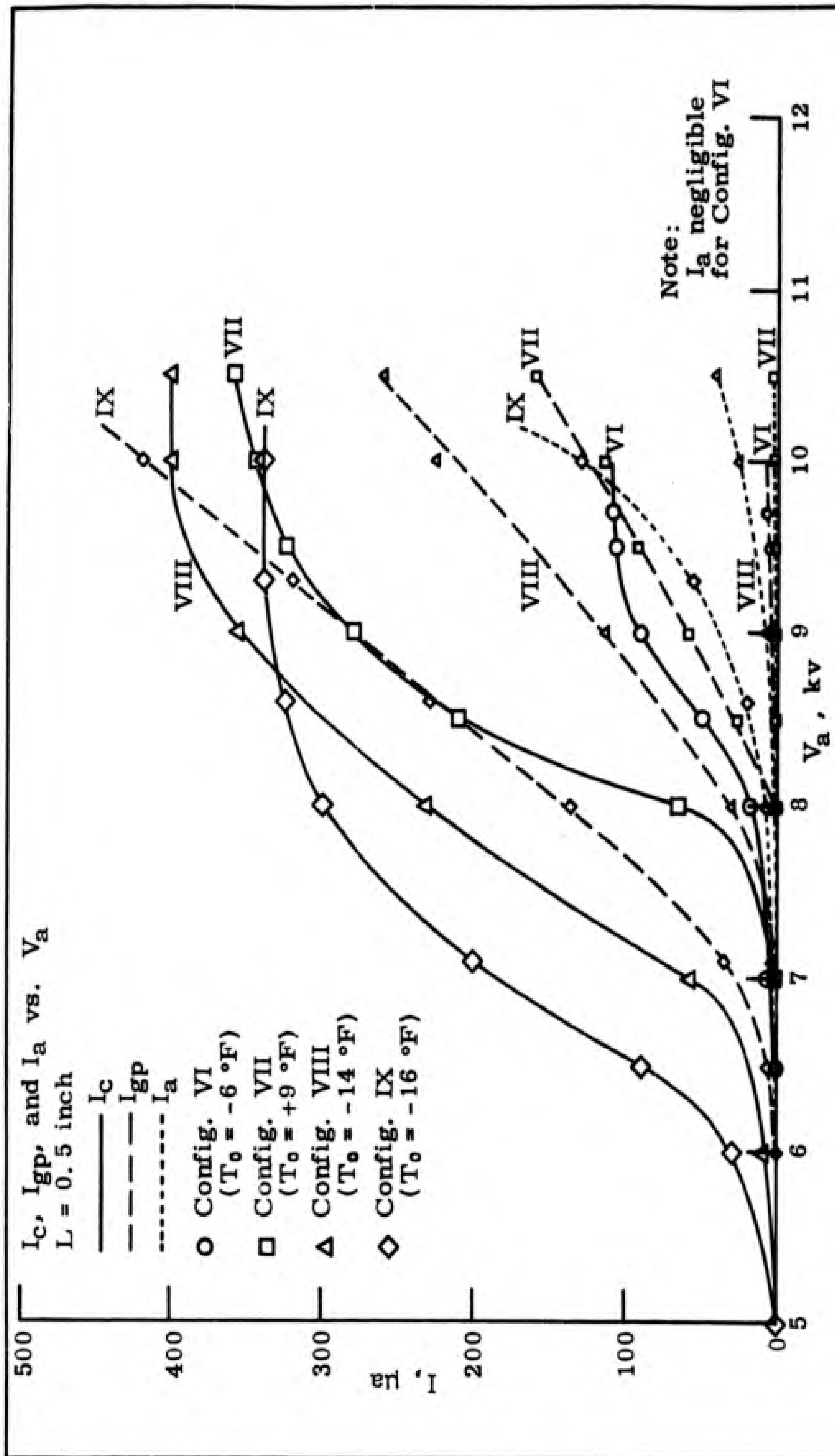

FIGURE 18

Current Characteristics for Configurations VI, VII, VIII, and IX (P_o = 150 psig)

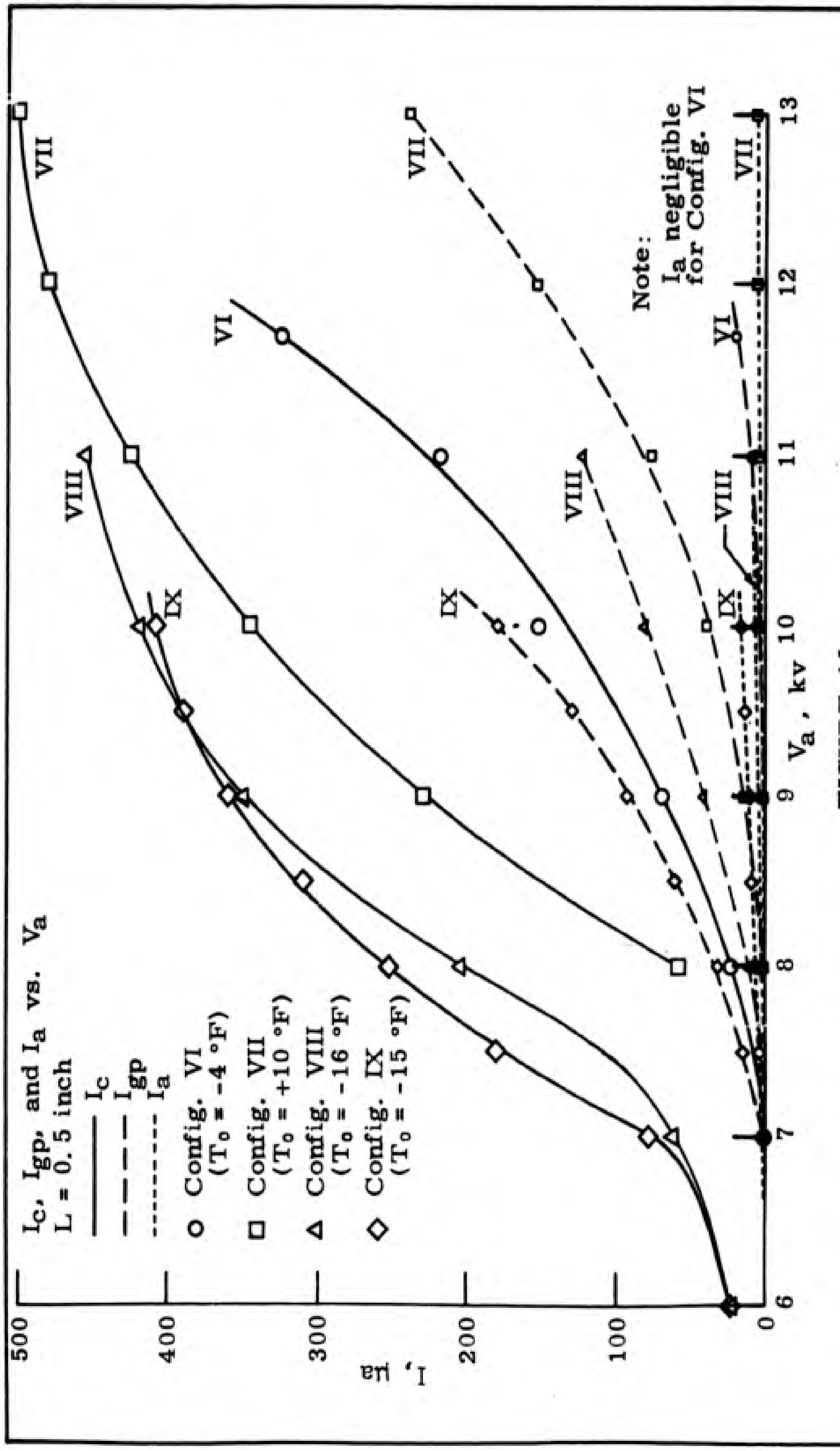

FIGURE 19

Current Characteristics for Configurations VI, VII, VIII, and IX (P_o = 200 psig)

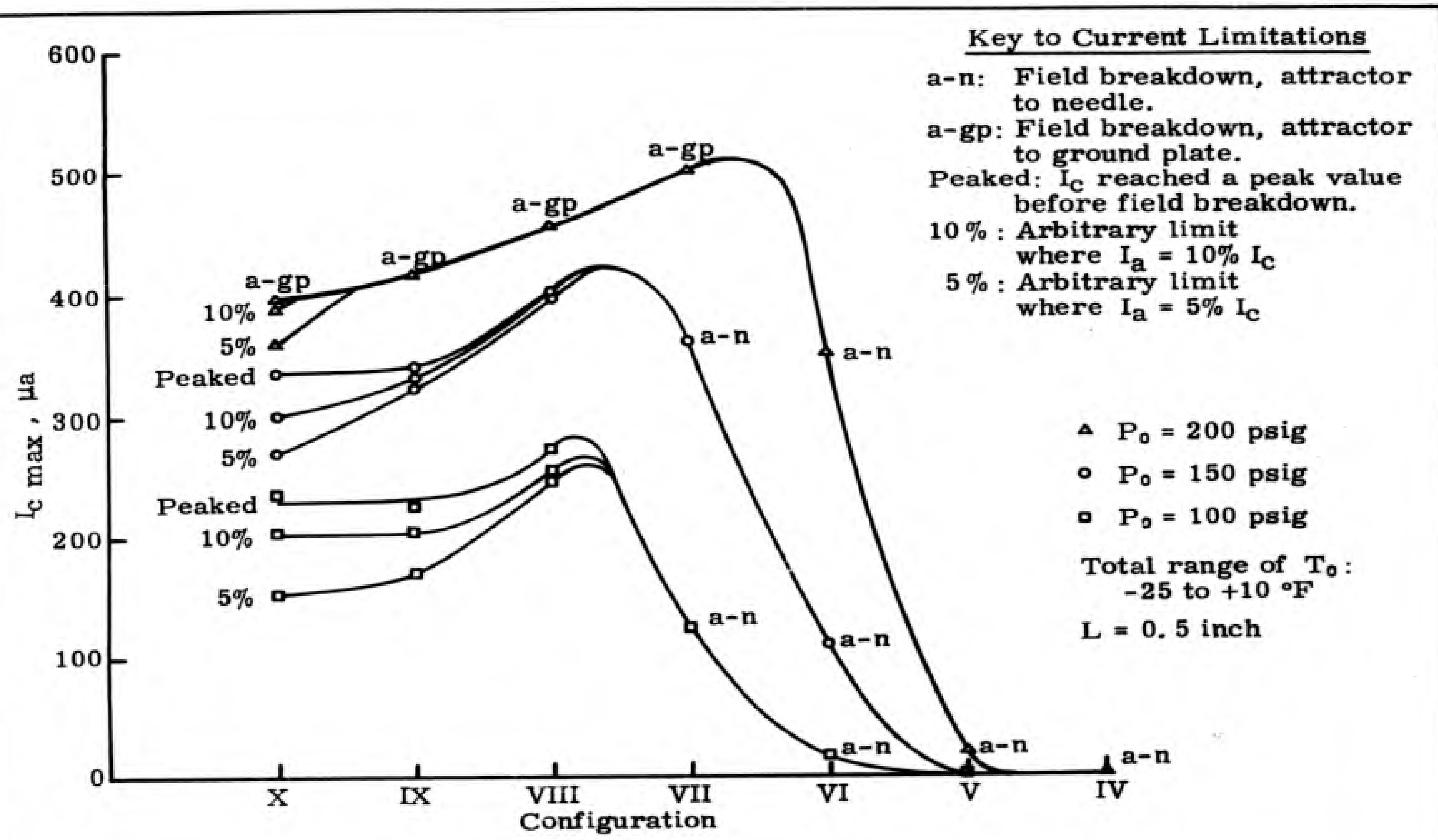

FIGURE 20
Effect of Needle Position on Maximum Collector Current Obtained

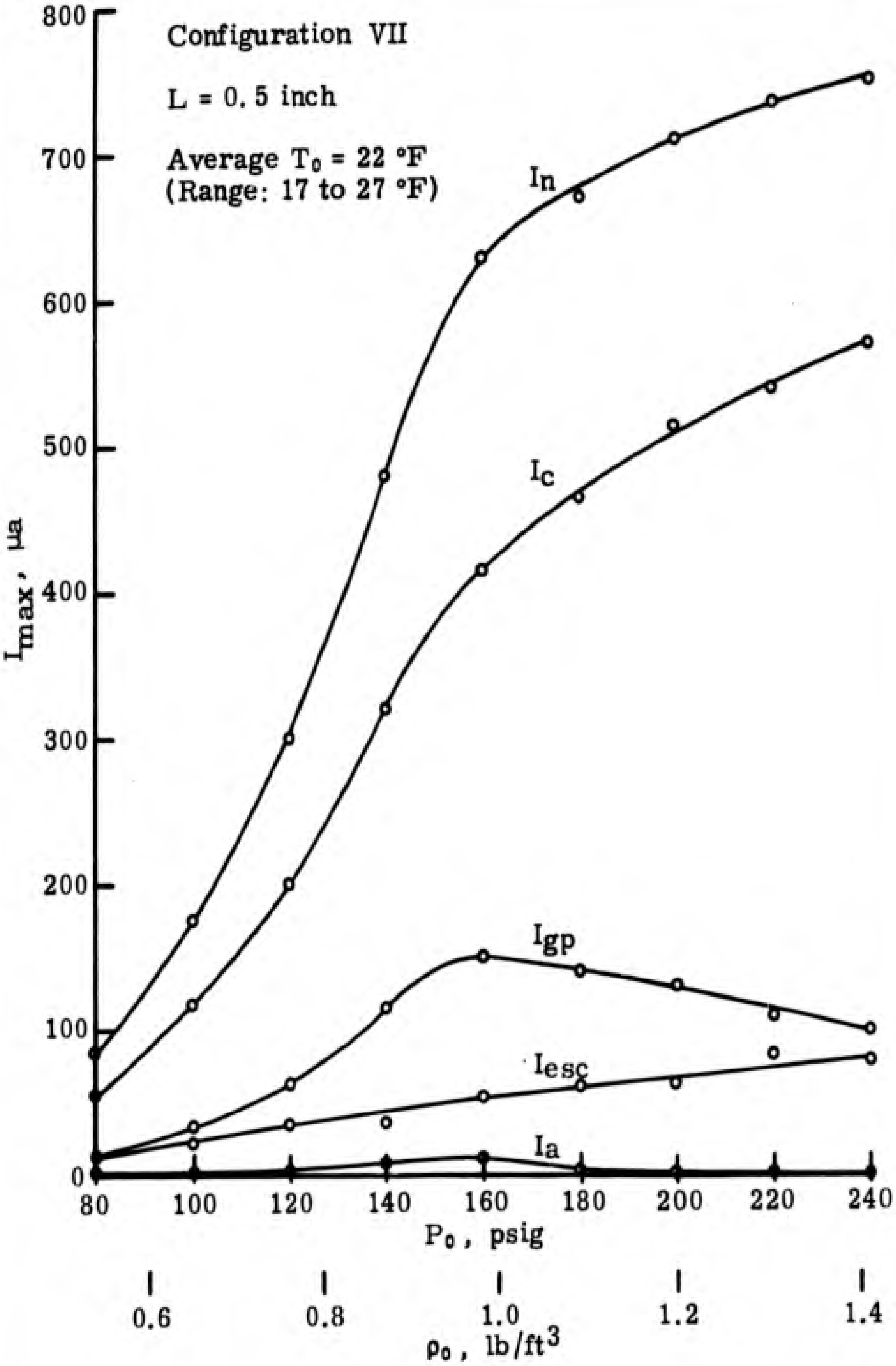

FIGURE 21

Effect of Pressure (or Density) on Maximum Currents Obtained

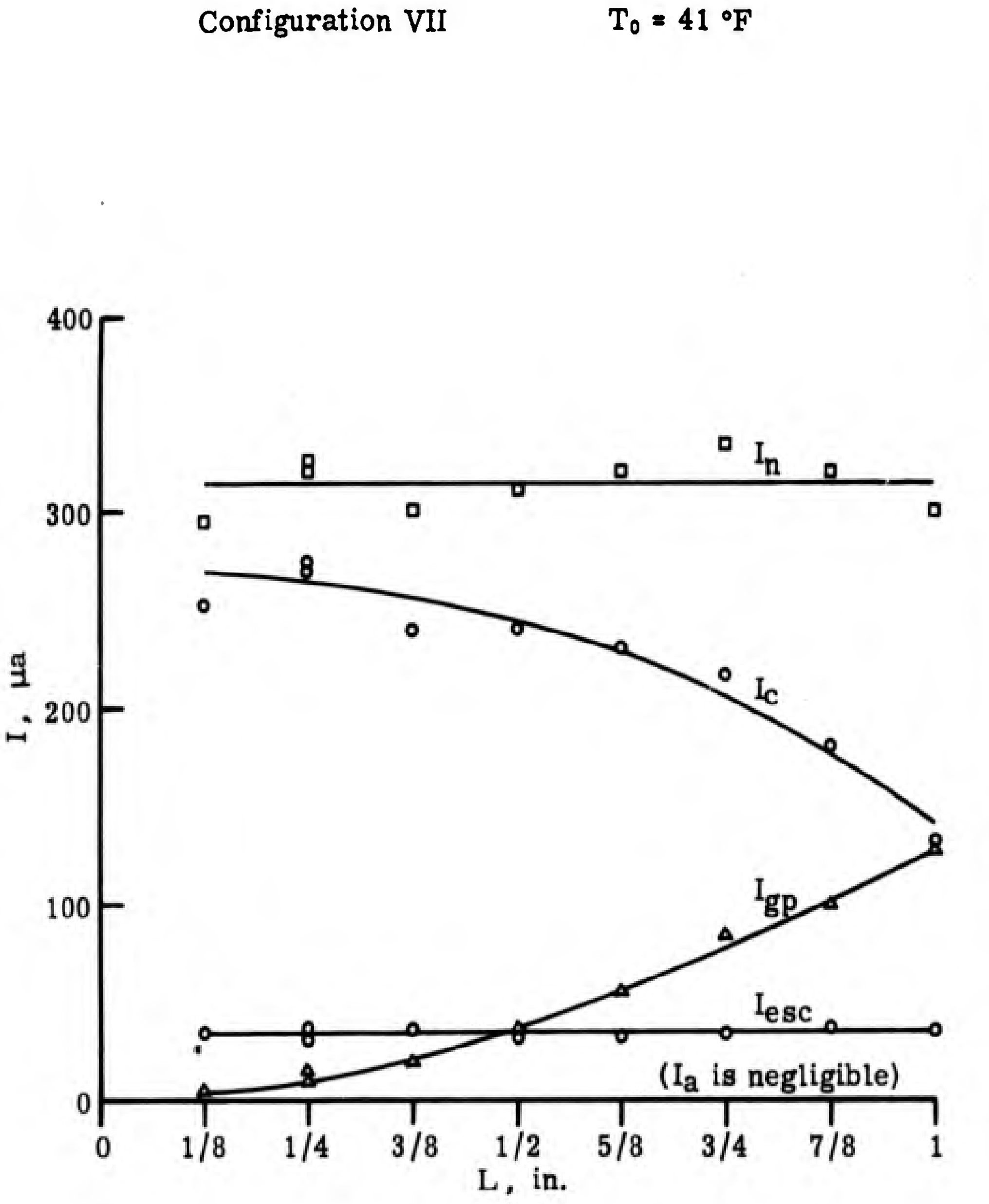

FIGURE 22

Effect of Length of Transport Region on Maximum Currents Obtained (P_0 = 150 psig)

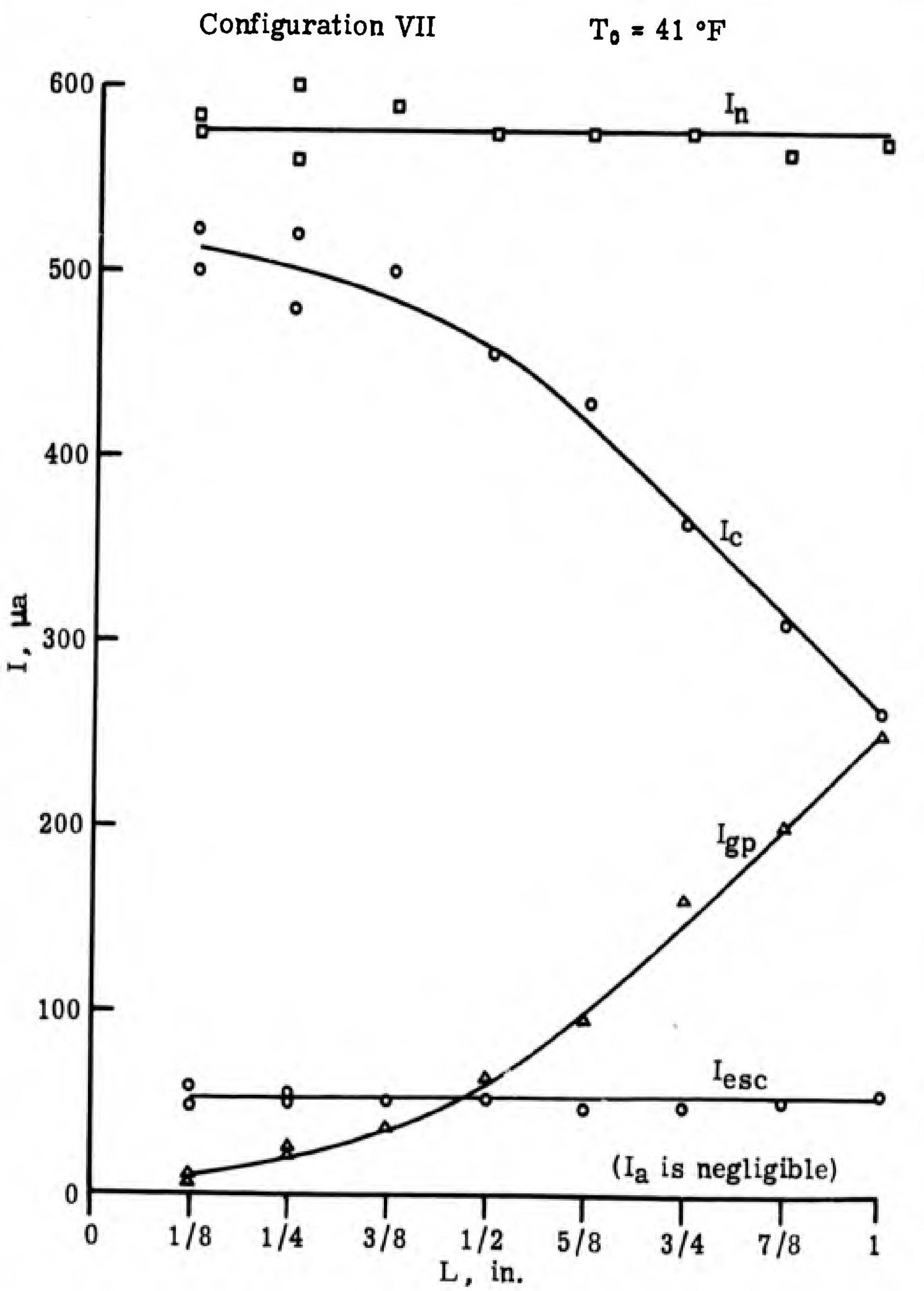

FIGURE 23

Effect of Length of Transport Region on Maximum Currents Obtained (P_0 = 200 psig)

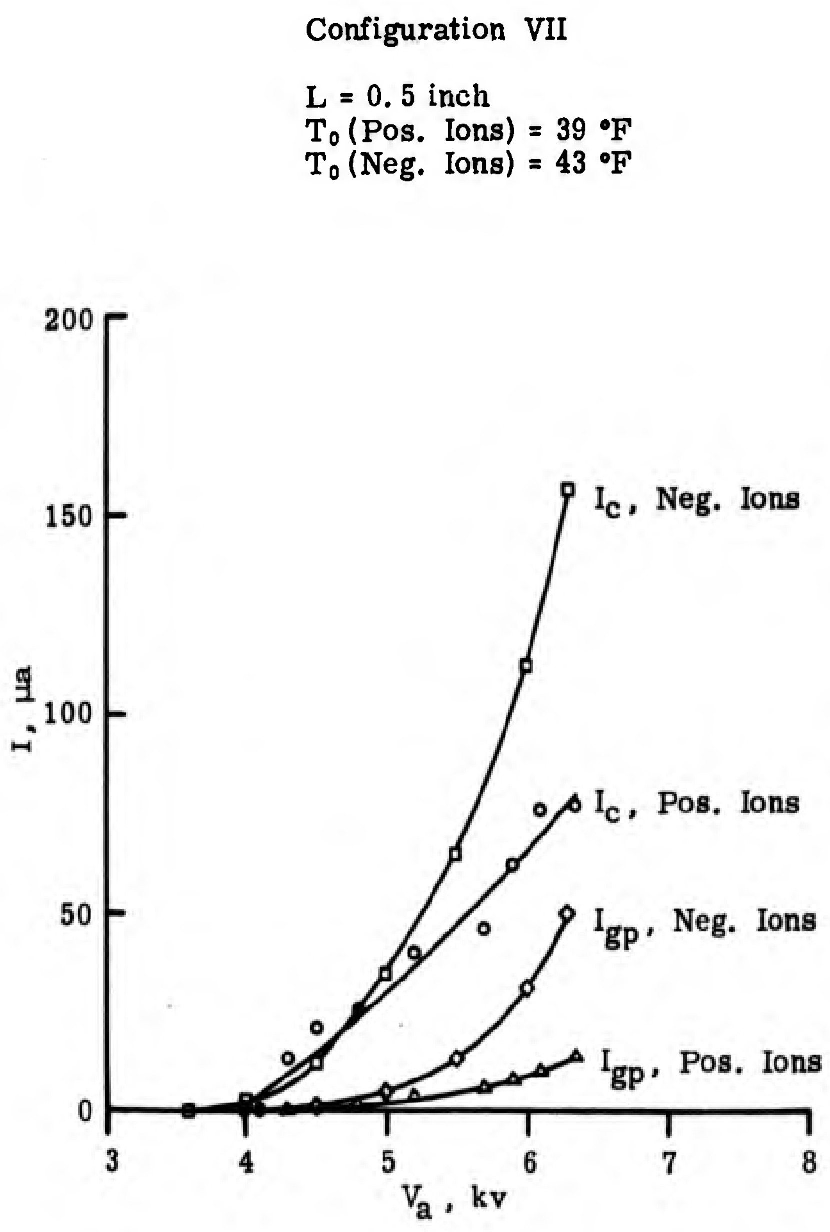

FIGURE 24

Comparison of Current Characteristics for Positive and Negative Ion Flow (P_0 = 100 psig)

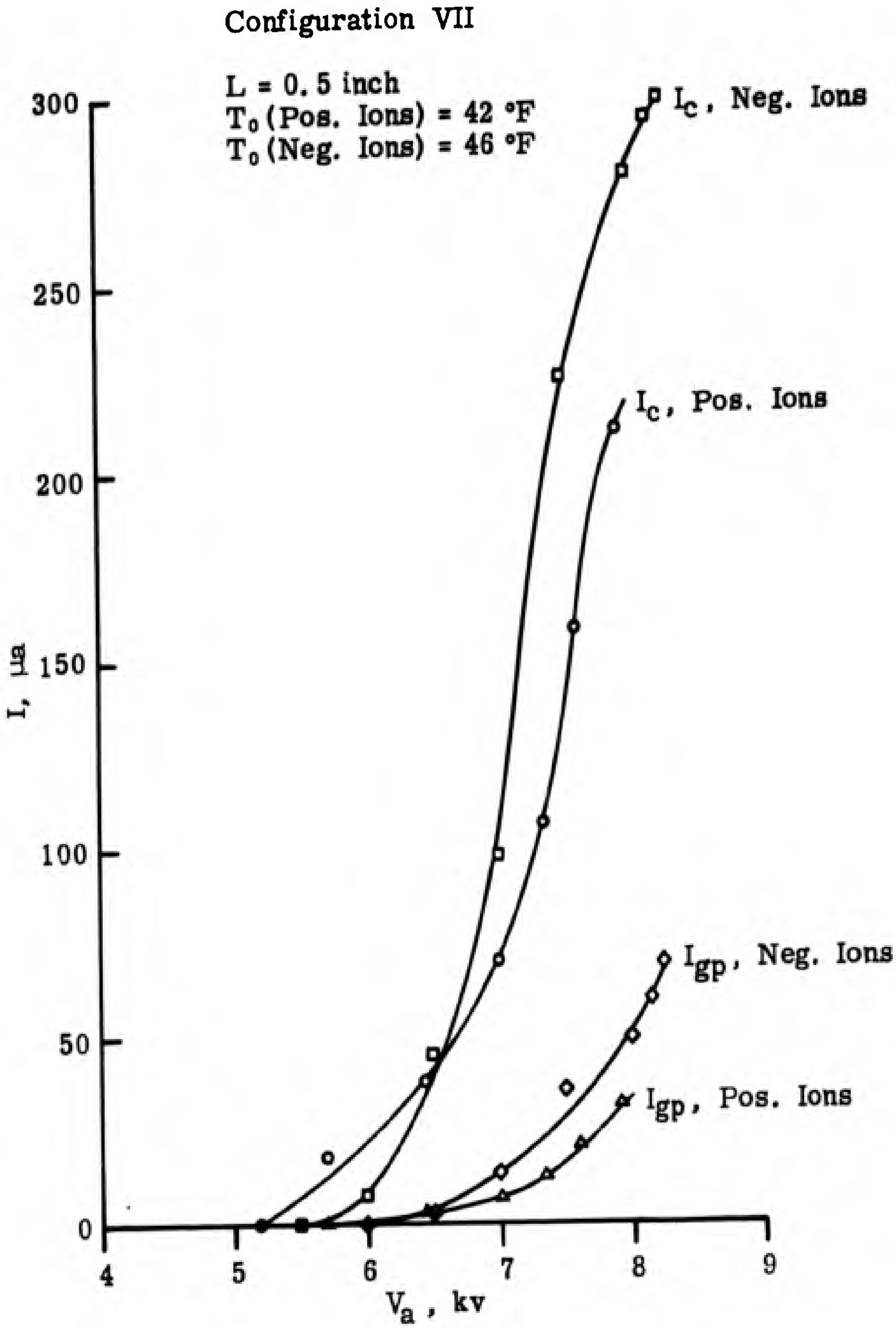

FIGURE 25

Comparison of Current Characteristics for Positive and Negative Ion Flow (P_0 = 150 psig)

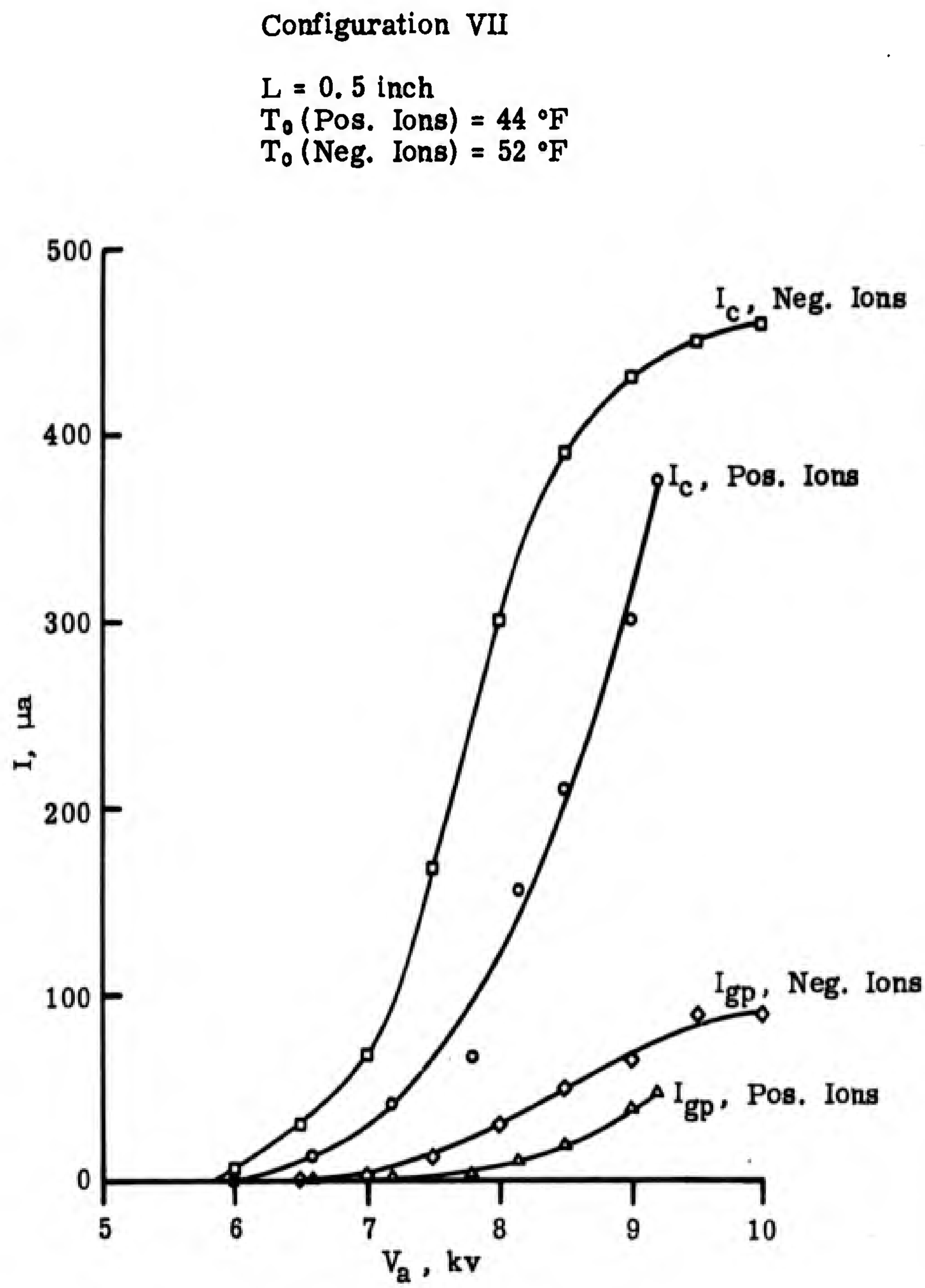

FIGURE 26

Comparison of Current Characteristics
for Positive and Negative Ion Flow
(P_0 = 200 psig)

TABLE I

Areas and Area Ratios of the Nozzle Configurations

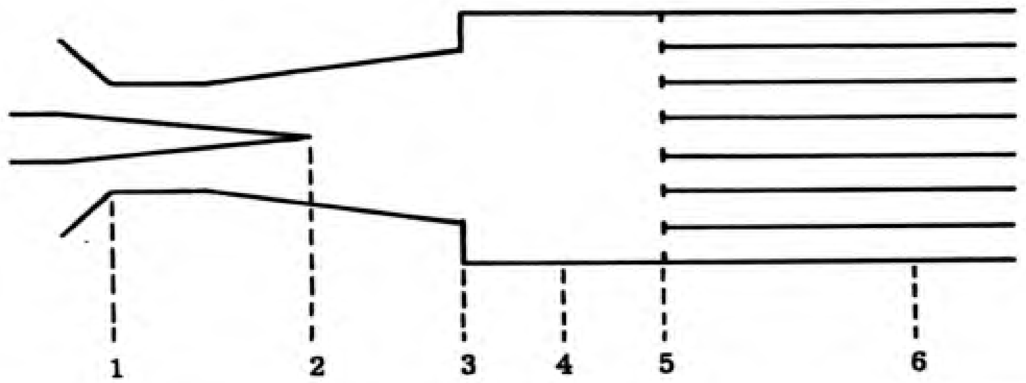

Configuration	I	II	III	IV	V	VI	VII	VIII	IX	X
A_1 (one nozzle)	0.0101	0.0105	0.0109	0.0109	0.0112	0.0115	0.0117	0.0119	0.0121	0.0122
A_2 (one nozzle)	0.0170	0.0163	0.0155	0.0142	0.0135	0.0129	0.0129	0.0129	0.0123	0.0123
A_3 (one nozzle)	0.0170	0.0170	0.0170	0.0170	0.0170	0.0170	0.0170	0.0170	0.0170	0.0170
A_1 (total)	0.254	0.264	0.273	0.273	0.280	0.288	0.294	0.298	0.302	0.305
A_2 (total)	0.424	0.406	0.389	0.355	0.338	0.322	0.322	0.322	0.307	0.307
A_3 (total)	0.424	0.424	0.424	0.424	0.424	0.424	0.424	0.424	0.424	0.424
A_2/A_1	1.67	1.54	1.42	1.30	1.21	1.12	1.10	1.08	1.02	1.01
A_3/A_1	1.67	1.61	1.55	1.55	1.51	1.47	1.44	1.42	1.40	1.39

A_4 = 0.988 for all configurations
A_5 = 0.391 for all configurations
A_6 = 0.751 for all configurations

(All areas are given in square inches)

TABLE II

Nozzle Flow Parameters, Configuration VII

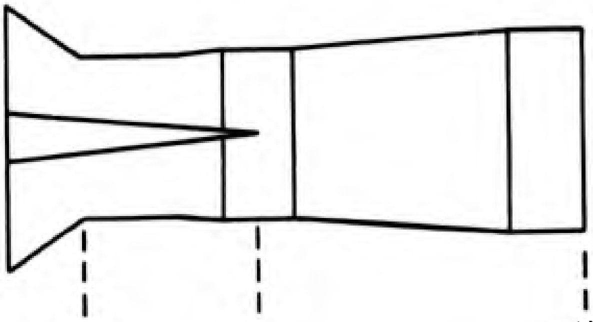

P_0	(psig)	100	150	200
T_0	(°R)	460	460	460
ρ_0	(lbm/ft^3)	0.675	0.969	1.262
M_1		1.00	1.00	1.00
M_2		1.36	1.36	1.36
M_3		1.80	1.80	1.80
T_2	(°R)	336	336	336
T_3	(°R)	279	279	279
v_2	(ft/sec)	1220	1220	1220
v_3	(ft/sec)	1480	1480	1480
$v_{avg(2-3)}$	(ft/sec)	1350	1350	1350
ρ_2	(lbm/ft^3)	0.307	0.441	0.575
ρ_3	(lbm/ft^3)	0.194	0.278	0.362
$\rho_{avg(2-3)}$	(lbm/ft^3)	0.250	0.360	0.468
$\dot{m}$	(lbm/sec)	0.84	1.21	1.57

TABLE III

Total Pressure, Density, and Needle Current Relations from Figure 21

P_0 psig	ρ_0 lbm/ft^3	I_n μa	I_n/ρ_0 $\mu a/(lbm/ft^3)$
80	0.53	80	150
100	0.64	180	280
120	0.76	300	390
140	0.87	490	560
160	0.98	630	640
180	1.09	680	620
200	1.20	710	590
220	1.32	730	550
240	1.43	750	520

TABLE IV

Comparison of Positive and Negative Ion Flows

(Configuration VII)

	Polarity of ions	Total Pressure, psig 100	150	200
I_c max (μa)	+	80	220	375
	-	156	300	460
I_{gp} max (μa)	+	14	34	48
	-	50	70	90
I_{gp}/I_c	+	0.175	0.155	0.128
	-	0.320	0.233	0.196
V_a max (volts)	+	6350	8000	9200
	-	6300	8250	10,000

Appendix B

Complete Engineering Drawings for the EHD Generator

The first four drawings in this appendix (RN-61-D-979, RN-61-C-980, RN-61-A-980-6A, and RN-61-B-981) show the EHD generator as it was originally designed by the Aeronautical Research Laboratory. The other drawing (RN-62-C-1094) indicates changes which were made by this author and Captain Wheeler during their concurrent work with the generator.

[redacted]

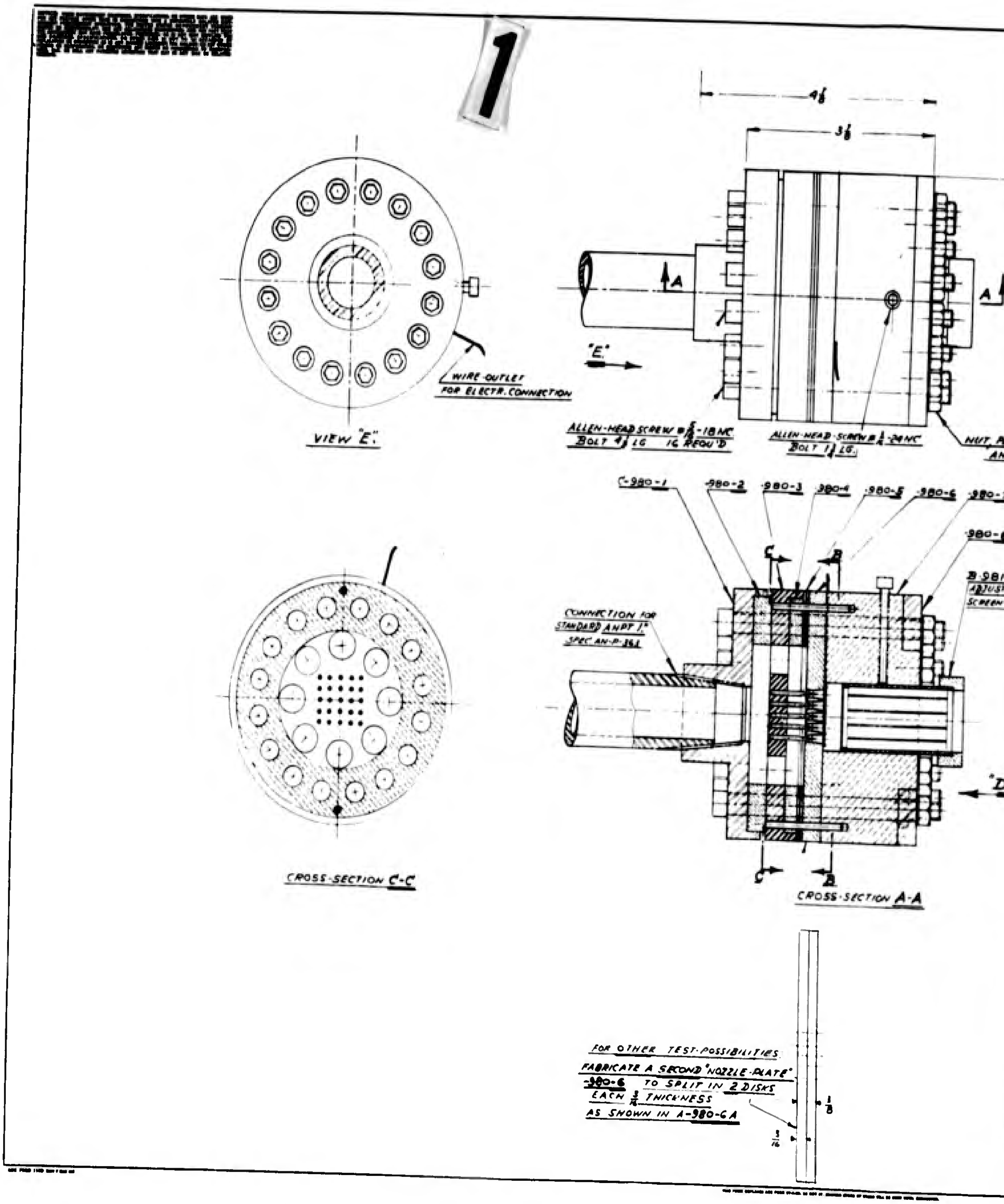

VIEW "E"
WIRE OUTLET FOR ELECTR. CONNECTION
"E"
ALLEN-HEAD SCREW
ALLEN-HEAD SCREW
C-980-1
980-2
980-3
980-4
980-5
980-6
CONNECTION FOR STANDARD ANPT 1" SPEC AN-P-361
CROSS-SECTION C-C
CROSS-SECTION A-A
FOR OTHER TEST-POSSIBILITIES
FABRICATE A SECOND "NOZZLE-PLATE" -980-6 TO SPLIT IN 2 DISKS EACH 3/16 THICKNESS
AS SHOWN IN A-980-6A

2

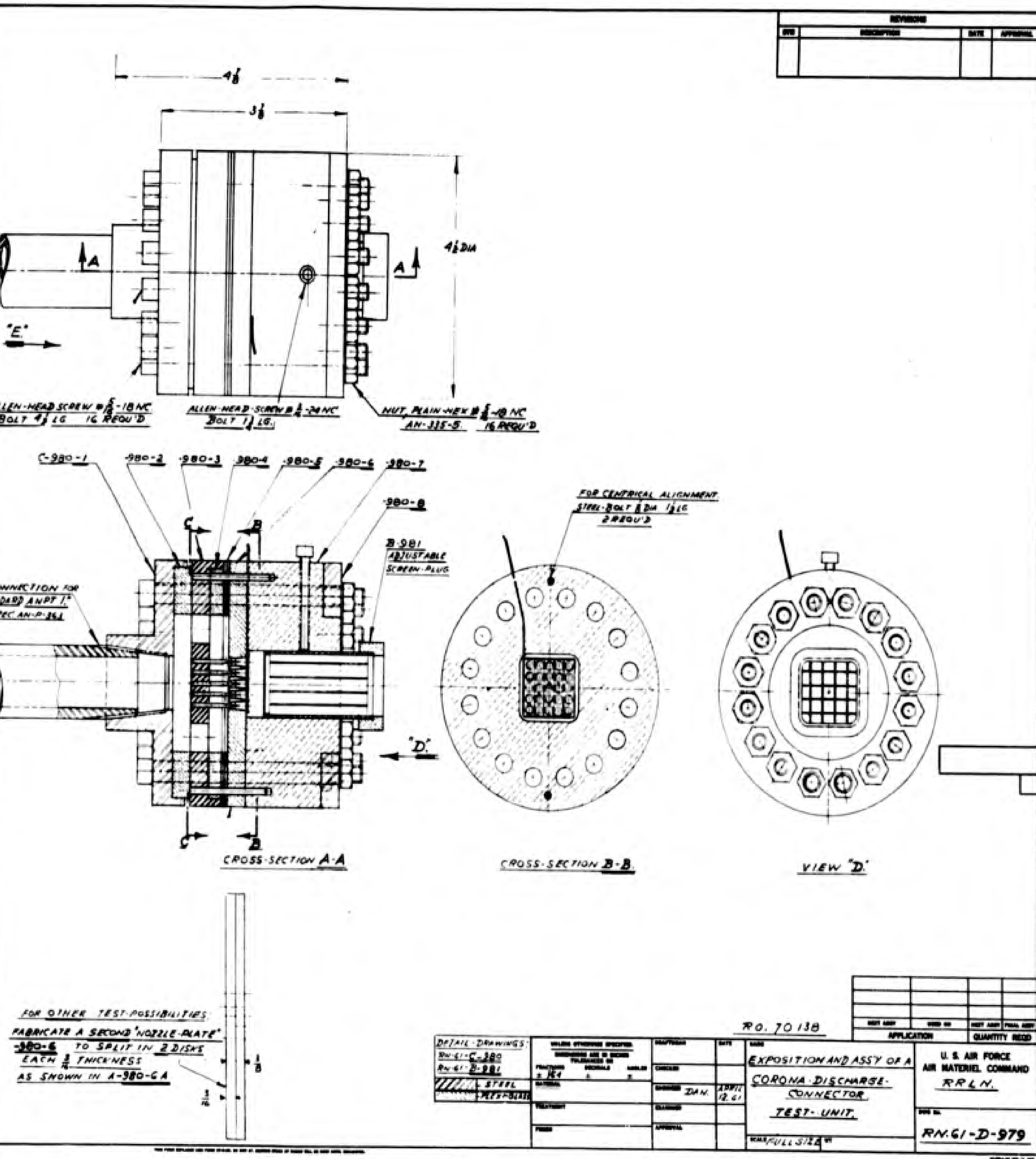
REVISIONS
DESCRIPTION
DATE
APPROVAL
4 1/8
3 1/8
4 1/2 DIA
A
A
"E"
ALLEN-HEAD SCREW # 5/16 -18 NC BOLT 4 1/2 LG 16 REQU'D
ALLEN-HEAD-SCREW # 1/4 -24 NC BOLT 1 1/4 LG.
NUT, PLAIN-HEX # 5/16 -18 NC AN-315-5. 16 REQU'D
C-980-1
-980-2
-980-3
-980-4
-980-5
-980-6
-980-7
-980-8
B-981 ADJUSTABLE SCREEN-PLUG
C
B
C
B
"D"
FOR CENTRICAL ALIGNMENT STEEL-BOLT 1/8 DIA 1/2 LG 2 REQU'D
CROSS-SECTION A-A
CROSS-SECTION B-B
VIEW "D"
FOR OTHER TEST-POSSIBILITIES: FABRICATE A SECOND "NOZZLE-PLATE" -980-6 TO SPLIT IN 2 DISKS EACH 1/8 THICKNESS AS SHOWN IN A-980-6 A
1/8
1/16
RO. 70138
APPLICATION
QUANTITY REQD
DETAIL-DRAWINGS:
RN-61-C-980
RN-61-B-981
STEEL
PLEXI-GLASS
± 1/64
DAN.
APRIL 12. 61
EXPOSITION AND ASSY OF A CORONA-DISCHARGE-CONNECTOR TEST-UNIT.
U. S. AIR FORCE
AIR MATERIEL COMMAND
RRLN.
FULL SIZE
RN.61-D-979

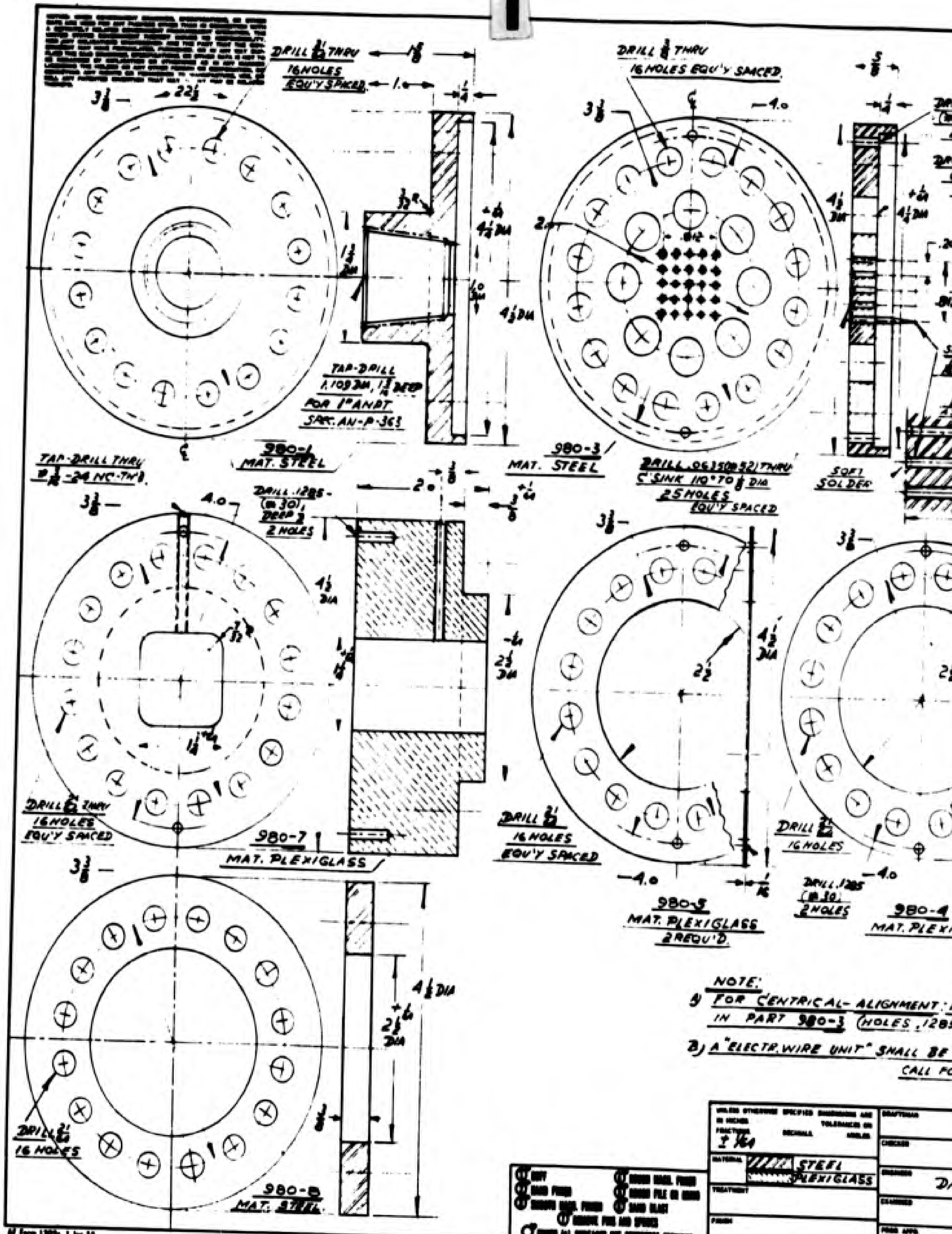
DRILL 21/64 THRU 16 HOLES EQU'Y SPACED
TAP-DRILL 1.109 DIA, 1 3/4 DEEP FOR 1" ANPT SPEC. AN-P-363
980-1
MAT. STEEL
DRILL 3/8 THRU 16 HOLES EQU'Y SPACED
980-3
MAT. STEEL
DRILL .0635 (#52) THRU C'SINK 110° TO 1/8 DIA 25 HOLES EQU'Y SPACED
SOFT SOLDER
TAP-DRILL THRU #10-24 NC-TH'D
DRILL .1285 (#30) DEEP 3/8 2 HOLES
980-7
MAT. PLEXIGLASS
DRILL 21/64 THRU 16 HOLES EQU'Y SPACED
DRILL 21/64 16 HOLES EQU'Y SPACED
980-5
MAT. PLEXIGLASS
2 REQU'D
DRILL 21/64 16 HOLES
DRILL .1285 (#30) 2 HOLES
980-4
MAT. PLEXI
DRILL 21/64 16 HOLES
980-8
MAT. STEEL
NOTE:
A) FOR CENTRICAL-ALIGNMENT
IN PART 980-3 (HOLES .128
B) A "ELECTR. WIRE UNIT" SHALL BE
CALL FO
STEEL
PLEXIGLASS
AF Form 1300c, 1 Jan 55

2

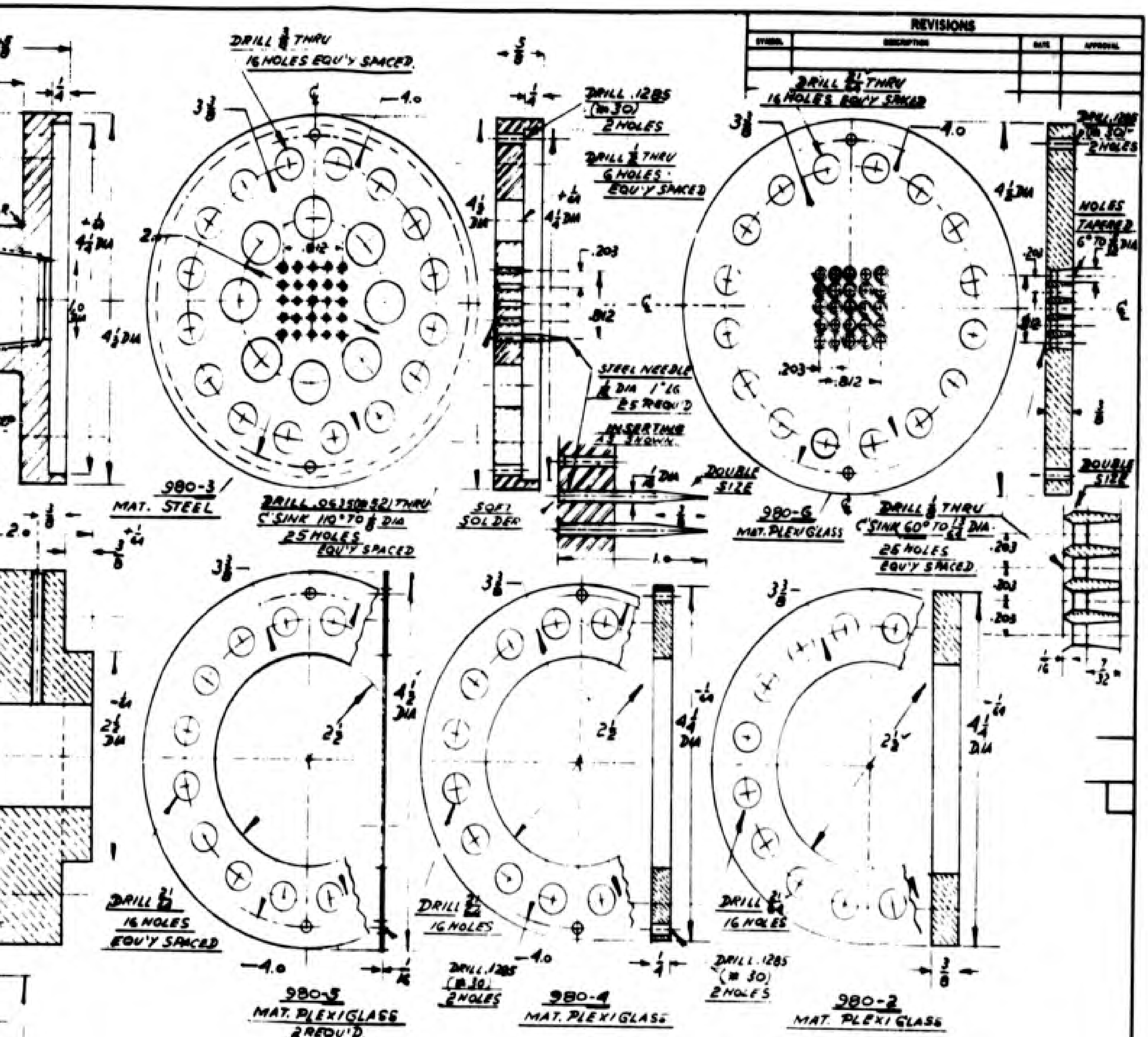

NOTE:

1) FOR CENTRICAL-ALIGNMENT: INSERT 2 BOLTS 1/8 DIA 1 1/2 LG IN PART 980-3 (HOLES .1285 DIA) SHOWN IN ASS'Y D-979

2) A "ELECTR. WIRE UNIT" SHALL BE PLACED AT PART 980-6 CALL FOR INFORMATION RRLN.

R.O. 70138

RN-61-D-979			
NEXT ASSY	USED ON	NEXT ASSY	FINAL ASSY
APPLICATION		QUANTITY REQD	

UNLESS OTHERWISE SPECIFIED DIMENSIONS ARE IN INCHES. TOLERANCES ON FRACTIONS ± 1/64

MATERIAL: STEEL / PLEXIGLASS

ENGINEER: DAN. — APRIL 14.61.

NAME: DETAILS FOR CORONA-DISCHARGE-CONNECTOR. RN-61-D-979, TEST-UNIT.

U. S. AIR FORCE RRLN.

SCALE: FULL SIZE

DRAWING NO. RN-61-C-980

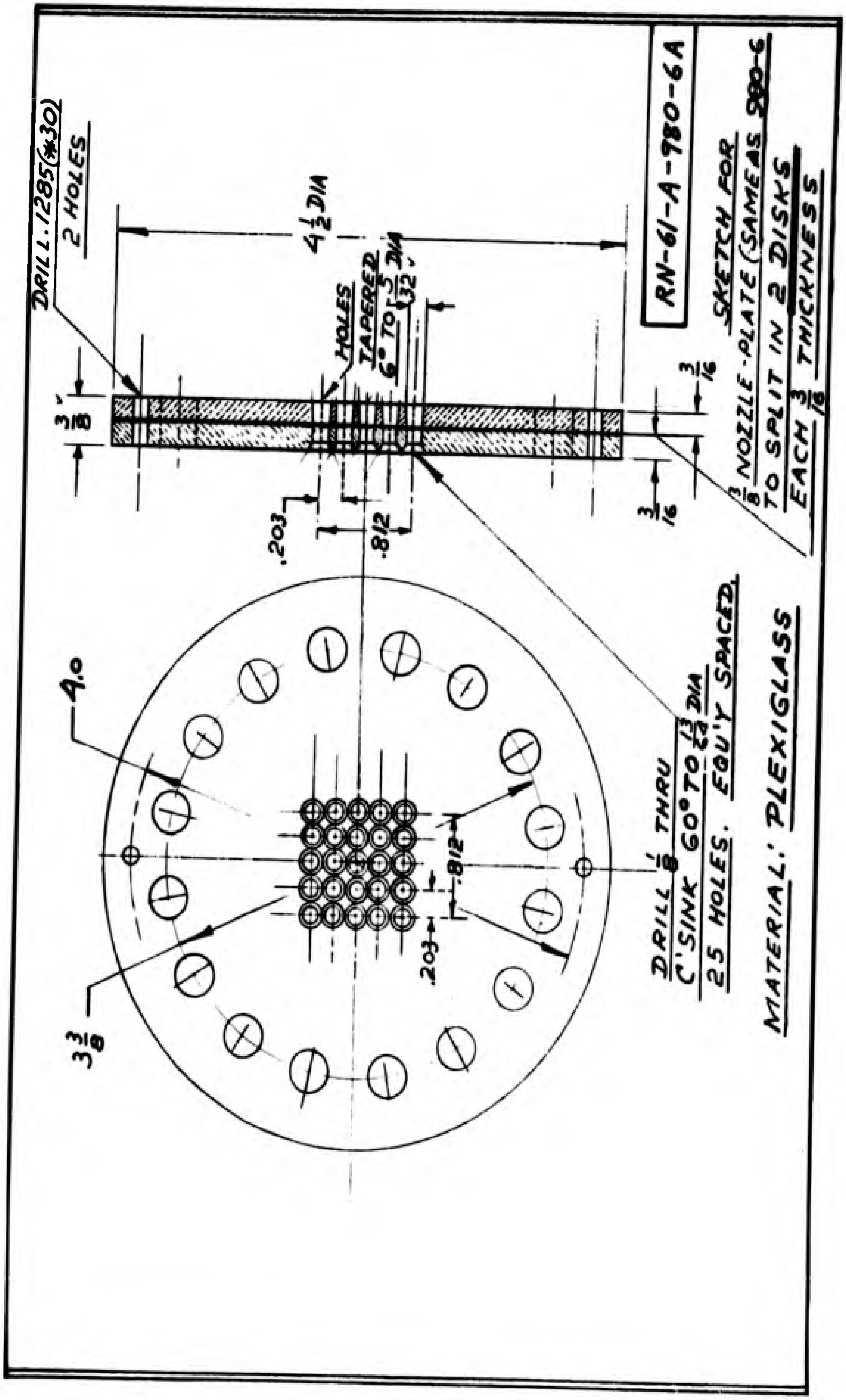

DRILL .1285(#30)
2 HOLES
$4\frac{1}{2}$ DIA
HOLES
TAPERED
6° TO $\frac{5}{32}$ DIA
$\frac{3}{8}$
.203
.812
$\frac{3}{16}$
$\frac{3}{16}$
RN-61-A-980-6A
SKETCH FOR
$\frac{3}{8}$ NOZZLE-PLATE (SAME AS 980-6
TO SPLIT IN 2 DISKS
EACH $\frac{3}{16}$ THICKNESS
4.0
$3\frac{3}{8}$
.812
.203
DRILL $\frac{1}{8}$ THRU
C'SINK 60° TO $\frac{13}{64}$ DIA
25 HOLES. EQU'Y SPACED.
MATERIAL: PLEXIGLASS

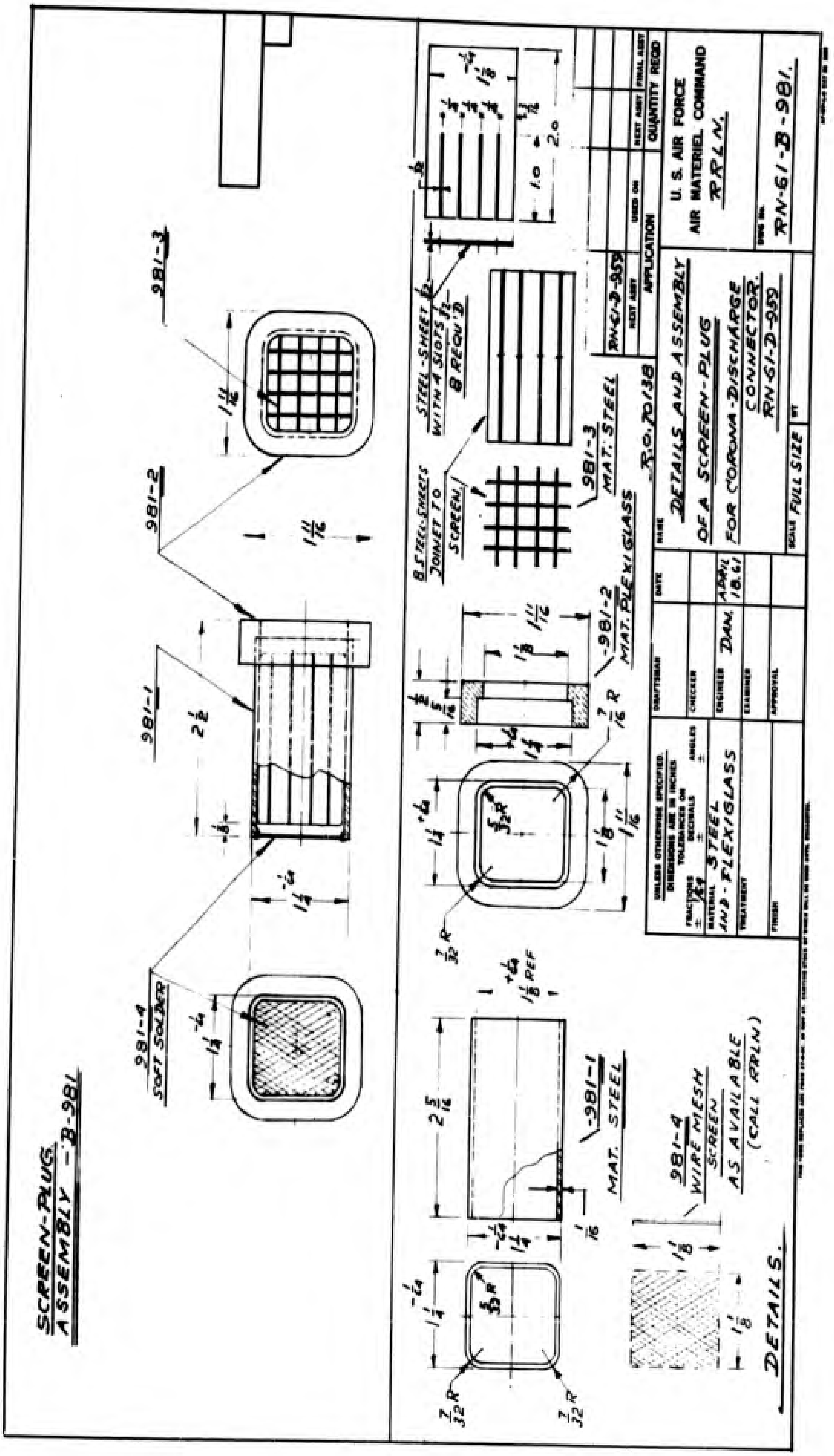
SCREEN-PLUG ASSEMBLY - B-981
981-4 SOFT SOLDER
981-1
981-2
981-3
DETAILS.
981-1 MAT. STEEL
981-4 WIRE MESH SCREEN AS AVAILABLE (CALL RRLN)
981-2 MAT. PLEXIGLASS
981-3 MAT: STEEL
8 STEEL-SHEETS JOINED TO SCREEN.
STEEL-SHEET WITH 4 SLOTS 8 REQU'D
R.O. 70138
RN-61-D-959
APPLICATION
QUANTITY REQD
U. S. AIR FORCE
AIR MATERIEL COMMAND
RRLN.
DETAILS AND ASSEMBLY OF A SCREEN-PLUG FOR CORONA-DISCHARGE CONNECTOR. RN-61-D-959
SCALE FULL SIZE
RN-61-B-981.
MATERIAL STEEL AND - FLEXIGLASS
ENGINEER DAN.
APRIL 18.61

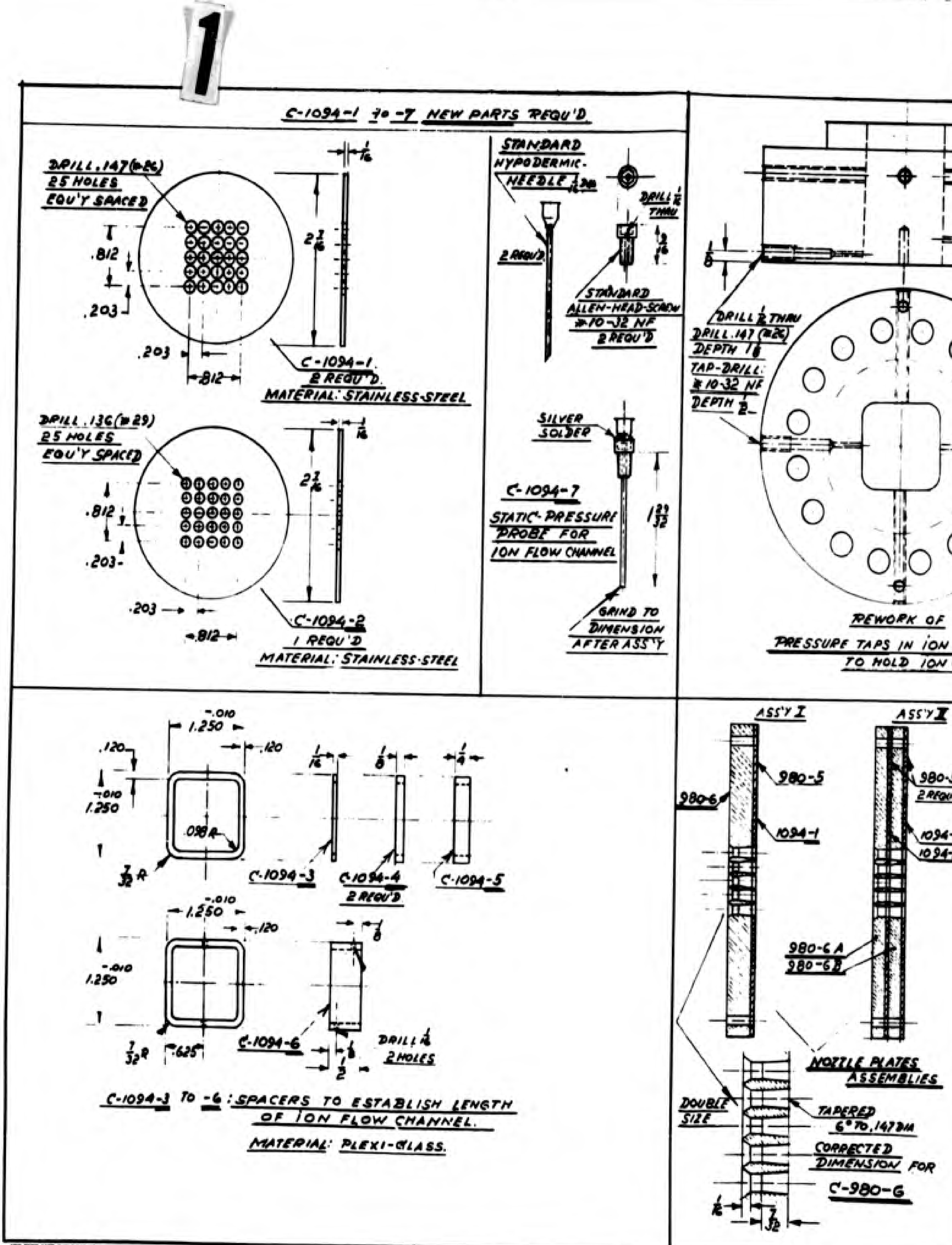
1
C-1094-1 TO -7 NEW PARTS REQU'D
DRILL .147 (#26) 25 HOLES EQU'Y SPACED
.812
.203
.203
.812
$2\frac{7}{16}$
$\frac{1}{16}$
C-1094-1 2 REQU'D MATERIAL: STAINLESS-STEEL
DRILL .136 (#29) 25 HOLES EQU'Y SPACED
.812
.203
.203
.812
$2\frac{7}{16}$
$\frac{1}{16}$
C-1094-2 1 REQU'D MATERIAL: STAINLESS-STEEL
STANDARD HYPODERMIC-NEEDLE
2 REQU'D
DRILL $\frac{1}{16}$ THRU
STANDARD ALLEN-HEAD-SCREW #10-32 NF 2 REQU'D
SILVER SOLDER
C-1094-7 STATIC-PRESSURE PROBE FOR ION FLOW CHANNEL
$1\frac{23}{32}$
GRIND TO DIMENSION AFTER ASS'Y
DRILL $\frac{1}{8}$ THRU
DRILL .147 (#26) DEPTH $1\frac{1}{8}$
TAP-DRILL #10-32 NF DEPTH $\frac{1}{2}$
REWORK OF
PRESSURE TAPS IN ION
TO HOLD ION
1.250 -.010
.120
.120
1.250 -.010
.098R
$\frac{7}{32}$R
$\frac{1}{16}$
$\frac{1}{8}$
$\frac{1}{4}$
C-1094-3
C-1094-4 2 REQU'D
C-1094-5
1.250 -.010
.120
$\frac{1}{8}$
1.250 -.010
$\frac{7}{32}$R
.625
C-1094-6
DRILL $\frac{1}{16}$ 2 HOLES
$\frac{1}{2}$
C-1094-3 TO -6: SPACERS TO ESTABLISH LENGTH OF ION FLOW CHANNEL.
MATERIAL: PLEXI-GLASS.
ASS'Y I
ASS'Y II
980-6
980-5
1094-1
980-6A
980-6B
2 REQU'D
NOZZLE PLATES ASSEMBLIES
DOUBLE SIZE
TAPERED 6° TO .147 DIA
CORRECTED DIMENSION FOR C-980-G
$\frac{1}{16}$
$\frac{7}{32}$

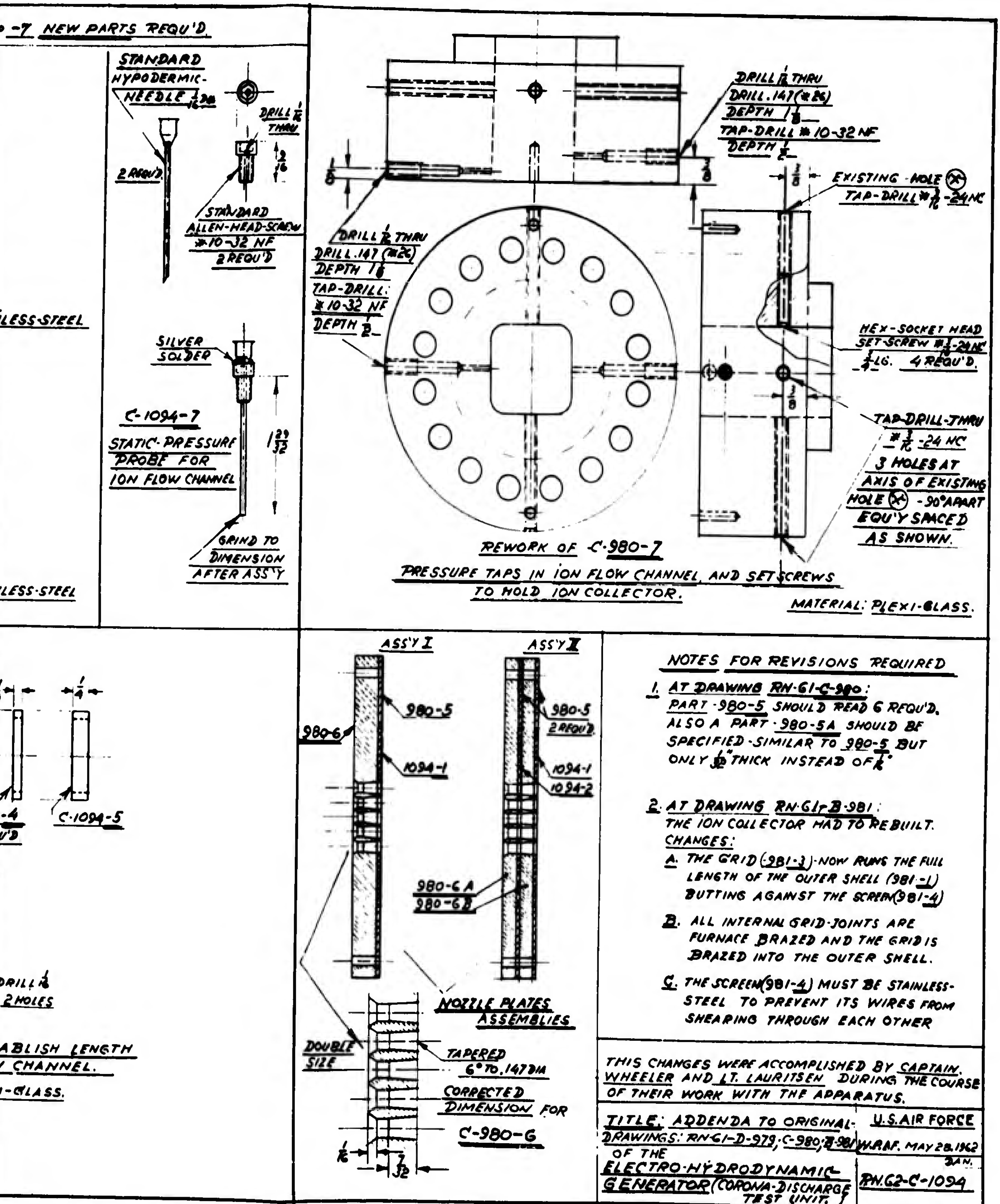
-7 NEW PARTS REQU'D.
STANDARD HYPODERMIC-NEEDLE 1/16 DIA
2 REQU'D.
DRILL 1/16 THRU
1/2 16
STANDARD ALLEN-HEAD-SCREW #10-32 NF 2 REQU'D
LESS-STEEL
SILVER SOLDER
C-1094-7
STATIC-PRESSURE PROBE FOR ION FLOW CHANNEL
1 29/32
GRIND TO DIMENSION AFTER ASS'Y
LESS-STEEL
DRILL 1/8 THRU
DRILL .147 (#26)
DEPTH 1/8
TAP-DRILL #10-32 NF
DEPTH 1/2
EXISTING HOLE (X)
TAP-DRILL # 1/16 -24NC
HEX-SOCKET HEAD SET-SCREW # 1/16 -24NC 1/4 LG. 4 REQU'D.
TAP-DRILL-THRU # 3/16 -24 NC
3 HOLES AT AXIS OF EXISTING HOLE (X) - 90° APART EQU'Y SPACED AS SHOWN.
REWORK OF C-980-7
PRESSURE TAPS IN ION FLOW CHANNEL AND SET SCREWS TO HOLD ION COLLECTOR.
MATERIAL: PLEXI-GLASS.
1/4
C-1094-5
-4
U'D
DRILL 1/16
2 HOLES
ABLISH LENGTH
CHANNEL.
-GLASS.
ASS'Y I
ASS'Y II
980-6
980-5
980-5 2 REQU'D.
1094-1
1094-1
1094-2
980-6A
980-6B
NOZZLE PLATES ASSEMBLIES
DOUBLE SIZE
TAPERED 6° TO .147 DIA
CORRECTED DIMENSION FOR C-980-6
1/16
7/32
NOTES FOR REVISIONS REQUIRED
1. AT DRAWING RN-61-C-980:
PART -980-5 SHOULD READ 6 REQU'D.
ALSO A PART -980-5A SHOULD BE SPECIFIED -SIMILAR TO 980-5 BUT ONLY 1/32" THICK INSTEAD OF 1/16"
2. AT DRAWING RN-61-B-981:
THE ION COLLECTOR HAD TO REBUILT.
CHANGES:
A. THE GRID (981-3) NOW RUNS THE FULL LENGTH OF THE OUTER SHELL (981-1) BUTTING AGAINST THE SCREEN (981-4)
B. ALL INTERNAL GRID-JOINTS ARE FURNACE BRAZED AND THE GRID IS BRAZED INTO THE OUTER SHELL.
C. THE SCREEN (981-4) MUST BE STAINLESS-STEEL TO PREVENT ITS WIRES FROM SHEARING THROUGH EACH OTHER
THIS CHANGES WERE ACCOMPLISHED BY CAPTAIN WHEELER AND LT. LAURITSEN DURING THE COURSE OF THEIR WORK WITH THE APPARATUS.
TITLE: ADDENDA TO ORIGINAL-DRAWINGS: RN-61-D-979, C-980, B-981 OF THE ELECTRO-HYDRODYNAMIC GENERATOR (CORONA-DISCHARGE TEST UNIT.)
U.S. AIR FORCE
W.R.A.F. MAY 28, 1962
RN 62-C-1094
2

Appendix C

Influence of the Attractor on the Ion Flow from the Corona

Problem

Considering only the field due to the attractor, an approximate equation is to be derived which will give the outside radius of the ion cloud as a function of the axial distance from the needle point. The result is to be valid only within the short cylinder defined by the attractor ring.

Assumptions

1. The field due to space charge is neglected.
2. The field due to the attractor is radial only, and exists only inside the cylindrical section (of radius r_a) defined by the attractor.
3. The grounded needle can be approximated by a grounded wire (of radius r_o) along the axis of the cylinder.
4. The gas velocity is axial only.
5. The gas velocity and density are constant over the length of the cylinder.
6. Induced magnetic fields are neglected.

Solution

The ions, once formed by the corona discharge, move downstream with the same axial velocity v as the gas, because there is no axial electric field to affect them. Their radial velocity, u_r, is given by

$$u_r = k\, E_r \tag{C-1}$$

where k is the ion mobility, and E_r is the radial electric field which will now be derived.

Since the space charge is being neglected for the present, Laplace's equation is valid:

$$\nabla^2 V = 0 \qquad \text{(C-2)}$$

where V is the electric potential.

With the restrictions and symmetry of this problem, the operation $\nabla^2 V$ in cylindrical coordinates reduces to $\frac{1}{r}\frac{d}{dr}(r\,dV/dr)$; therefore, Eq (C-2) becomes

$$\frac{d}{dr}(r\,dV/dr) = 0 \qquad \text{(C-3)}$$

or

$$r\,dV/dr = C \qquad \text{(C-4)}$$

where C is a constant of integration.

Rearranging Eq (C-4),

$$dV = C\,dr/r \qquad \text{(C-5)}$$

and integration from r_o to r and V_n to V yields

$$V - V_n = C \ln(r/r_o) \qquad \text{(C-6)}$$

Since the needle is grounded (i.e. $V_n = 0$), the boundary condition of the attractor voltage ($V = V_a$ at $r = r_a$) results in

$$C = \frac{V_a}{\ln(r_a/r_o)} \qquad \text{(C-7)}$$

Substitution of Eq (C-7) into Eq (C-6), with $V_n = 0$, yields a general expression for V:

$$V = \frac{V_a}{\ln(r_a/r_o)} \ln(r/r_o) \tag{C-8}$$

Now, in general, $\bar{E} = -\nabla V$, where $\bar{E}$ is the electric field intensity vector. In the simplified cylindrical coordinates of this problem, this reduces to

$$E_r = - dV/dr \tag{C-9}$$

The desired expression for E_r is obtained by substituting Eq (C-8) into Eq (C-9) and performing the differentiation:

$$E_r = \frac{-V_a}{\ln(r_a/r_o)} (1/r) \tag{C-10}$$

This expression for E_r can be used in Eq (C-1), giving the radial velocity of an ion:

$$u_r = \frac{-k\, V_a}{\ln(r_a/r_o)} (1/r) \tag{C-11}$$

Since $u_r = dr/dt$, Eq (C-11) can be written as

$$dr/dt = \frac{-k\, V_a}{\ln(r_a/r_o)} (1/r) \tag{C-12}$$

or

$$r\, dr = \frac{-k\, V_a}{\ln(r_a/r_o)} dt \tag{C-13}$$

Time can be related to the axial distance from the needle point, x, by the axial velocity v:

$$dt = dx/v \tag{C-14}$$

With the substitution of Eq (C-14) for dt, Eq (C-13) becomes

$$r\,dr = \frac{-k\,V_a}{v\,\ln(r_a/r_o)}\,dx \tag{C-15}$$

which can be integrated from r_i (the initial radial position of an ion) to r_x (the radial position at station x) and from 0 to x:

$$r_x^{\,2} = r_i^{\,2} - \frac{2\,k\,V_a}{v\,\ln(r_a/r_o)}\,x \tag{C-16}$$

This, then, is the required approximate equation for the effect of the attractor on the radius of the ion cloud at station x. (It has been derived for the motion of a <u>positive</u> ion, so that V_a is a <u>negative</u> potential. If V_a is positive, the sign of the fraction must be changed.) It shows that the ion cloud expands within the attractor region in the shape of a section of a paraboloid of revolution whose axis is the axis of the attractor ring.

Appendix D

Influence of the Space Charge on the Ion Flow from the Corona

Problem

Considering only the field due to the space charge, an approximate equation is to be derived which will give the outside radius of the ion stream as a function of the axial distance from the needle point. The result is to be valid throughout the nozzle.

Assumptions

1. The gas velocity is axial only.
2. The gas velocity and density are constant over the length of the nozzle.
3. The charge density is constant over any one cross section of the expanding ion cloud.
4. The ion stream is nearly cylindrical; thus the electric field due to the space charge is radial only.
5. The field due to the attractor is neglected.
6. Induced magnetic fields are neglected.

Solution

As stated in Appendix C, the ions, once formed by the corona, move downstream with the same axial velocity v as the gas, because there is no axial electric field to affect them. Their radial velocity, u_r, is given by

$$u_r = k\, E_r \tag{D-1}$$

where k is the ion mobility, and E_r is the radial electric field which will now be derived.

The following is one of Maxwell's four electromagnetic equations, written for free space:

$$\text{Divergence } \bar{E} = \rho_e/e_o \tag{D-2}$$

where $\bar{E}$ is the electric field intensity vector, ρ_e is the charge density, and e_o is the permittivity of free space.

Since $e_{air}/e_o = 1.0006$, Eq (D-2) is a very good approximation for air.

With the restrictions and symmetry of this problem, divergence $\bar{E}$ in cylindrical coordinates reduces to $(1/r)\,d/dr(r\,E_r)$. Eq (D-2) then becomes

$$(1/r)\; d/dr(r\,E_r) = \rho_e/e_o \tag{D-3}$$

or

$$d(r\,E_r) = (\rho_e/e_o)\; r\,dr \tag{D-4}$$

Since ρ_e is not a function of r within the ion cloud (by assumption 3), both sides of Eq (D-4) can be directly integrated from 0 to the outside radius of the ion cloud, r_x.

$$r_x E_r = (\rho_e/e_o)\; r_x^{\,2}/2 \tag{D-5}$$

or

$$E_r = (\rho_e/2\,e_o)\; r_x \tag{D-6}$$

This expression for E_r can be used in Eq (D-1), giving the radial velocity of an ion:

$$u_r = (k\,\rho_e / 2\,e_o)\,r_x \tag{D-7}$$

However, ρ_e must now be related to known constants and r_x. By continuity, it is known that

$$I_n/25 = \rho_e(\pi r_x^2)\,v \tag{D-8}$$

where $I_n/25$ is the needle current in one nozzle and πr_x^2 is the area of ion flow. Thus,

$$\rho_e = \frac{I_n/25}{\pi r_x^2\ v} \tag{D-9}$$

Substitution of Eq (D-9) into Eq (D-7) results in the following expression for u_r:

$$u_r = \frac{k\ I_n/25}{2\ e_o\ \pi\, r_x\ v} \tag{D-10}$$

Since $u_r = dr_x/dt$, Eq (D-10) can be written as

$$dr_x = \frac{k\ I_n/25}{2\ e_o\ \pi\, r_x\ v}\,dt \tag{D-11}$$

and since $dt = dx/v$, it becomes, with the variables separated,

$$r_x\,dr_x = \frac{k\ I_n/25}{2\ e_o\ \pi\, v^2}\,dx \tag{D-12}$$

It is fitting to discuss assumption 2, constant gas density and velocity in the nozzle, at this time. It is known that ρ decreases significantly in the nozzle (37%), and v increases a lesser amount (21%). However, since Eq (2), page 13, shows that k is inversely proportional to ρ, the real variable on the right hand side of Eq (D-12) is $1/\rho v^2$. This term is essentially constant, since the increase of v^2 approximately balances the decrease of ρ.

With the coefficient of dx considered constant, Eq (D-12) can be integrated from r_i, the initial radius of the cloud at the needle point, to r_x, and from 0 to x:

$$r_x^2/2 - r_i^2/2 = \frac{k\, I_n/25}{2\, e_o\, \pi v^2}\, x \qquad \text{(D-13)}$$

or

$$r_x^2 = r_i^2 + \frac{k\, I_n/25}{e_o\, \pi v^2}\, x \qquad \text{(D-14)}$$

Eq (D-14) is the required approximate equation for the effect of the space charge on the radius of the ion stream at station x. It shows that the ion stream takes the shape of a section of a paraboloid of revolution whose axis is the axis of the nozzle.

(A development similar to this can be found in Reference 7, pages 9 - 11.)

Appendix E

Tables of Original Experimental Data

In all tables of this appendix, the units are as follows:

Attractor potential	kv
All currents	μa
Total temperature	°F
Total pressure . . . . (Atmospheric pressure = 15 psia)	psig
Length of transport region	in.

TABLE V

Current Characteristic Data, Configuration I
(L = 0.50 inch)

V_a	I_a	I_c	T_0
	P_0 = 100 psig		
-2.50	0.0	0	8
-2.80	2.0	48	8
-3.00	5.0	80	9
-3.15	8.0	112	10
-3.25	13	134	10
-3.40	27	182	10
-3.50	57	210	10
-3.60	125	233	10
-3.70	228	234	10
	(No breakdown)		
	P_0 = 150 psig		
-3.00	0.0	0	13
-3.50	2.0	75	13
-3.83	5.0	134	13
-4.00	8.5	180	13
-4.20	24	268	13
-4.40	55	320	13
-4.60	128	360	13
-4.78	260	370	13
	(No breakdown)		
	P_0 = 200 psig		
-3.00	0.0	0	16
-3.90	1.3	74	16
-4.30	6.1	200	16
-4.50	9.4	234	16
-4.80	15	285	16
-5.10	35	400	16
-5.40	87	495	16
-5.60	172	544	16
-5.80	225	560	16
-5.95	250	580	16
-6.05	270	590	16
	(No breakdown)		

TABLE VI

Current Characteristic Data, Configuration II
(L = 0.50 inch)

V_a	I_a	I_c	T_0
	P_0 = 100 psig		
-2.00	0.0	0	10
-2.50	0.1	1	11
-3.00	2.0	16	13
-3.30	11	80	14
-3.50	35	166	15
-3.70	81	218	15
-3.90	195	235	15
-4.00	330	235	15
	(No breakdown)		
	P_0 = 150 psig		
-3.00	0.0	0	16
-3.50	0.7	17	17
-3.70	2.2	57	17
-4.00	6.0	108	18
-4.25	16	202	18
-4.50	35	293	18
-4.75	82	360	18
-5.00	195	385	18
-5.20	340	385	18
	(No breakdown)		
	P_0 = 200 psig		
-3.50	0.0	0	20
-4.00	0.3	13	20
-4.50	2.6	82	21
-4.90	8.0	166	21
-5.20	19	290	22
-5.50	50	440	22
-5.78	100	510	22
-6.00	170	540	22
-6.30	300	545	22
	(No breakdown)		

TABLE VII

Current Characteristic Data, Configuration III
(L = 0.50 inch)

V_a	I_a	I_c	T_0
	P_0 = 100 psig		
-3.10	0.0	0	16
-3.60	0.4	5	16
-4.03	10	42	16
-4.11	27	94	16
-4.23	65	168	16
-4.35	150	230	16
-4.43	215	240	16
-4.52	308	250	16
	(No breakdown)		
	P_0 = 150 psig		
-3.00	0.0	0	19
-3.50	0.1	5	19
-4.00	0.3	11	18
-4.50	1.3	27	18
-4.84	6.5	94	18
-5.00	11	139	18
-5.20	25	265	19
-5.60	66	380	19
-5.80	100	408	19
-6.18	200	415	19
-6.43	340	395	19
	(No breakdown)		
	P_0 = 200 psig		
-3.50	0.0	0	14
-4.00	0.1	5	14
-4.50	0.3	15	14
-5.00	0.6	90	15
-5.50	8.0	202	15
-6.00	16	310	15
-6.33	28	372	15
-6.65	50	455	15
-7.13	100	535	15
-7.62	190	565	15
-7.95	300	565	15
	(No breakdown)		

TABLE VIII

Current Characteristic Data, Configuration IV
(L = 0.50 inch)

V_a	I_a	I_{gp}	I_c	T_0
		P_0 = 100 psig		
-6.00	0.0	0	0	-16
-6.50	0.0	0	0	-16
-7.00	0.0	0	0	-16
-8.00	0.0	0	0	-16
-8.50	0.0	0	0	-16
-9.00	0.0	0	0	-16
-9.40	Breakdown, attractor to needle			
		P_0 = 150 psig		
-9.00	0.0	0	0	-14
-10.0	0.0	0	0	-14
-11.0	0.0	0	0	-13
-11.5	0.1	0	0	-12
-12.0	Breakdown, attractor to needle			
		P_0 = 200 psig		
-11.0	0.0	0	0	-10
-12.0	0.1	0	0	-10
-12.6	0.2	0	0	-10
-13.0	0.2	0	0	-10
-13.5	0.2	0	0	-10
-14.0	0.2	0	0	-10
-14.6	0.3	0	0	-10
-15.1	Breakdown, attractor to needle			

TABLE IX

Current Characteristic Data, Configuration V
(L = 0.50 inch)

V_a	I_a	I_{gp}	I_c	T_0
		P_0 = 100 psig		
-6.50	0.0	0	0	8
-7.00	0.0	0	0	8
-7.50	0.0	0	0	8
-7.90	Breakdown, attractor to needle			
		P_0 = 150 psig		
-7.50	0.0	0	0	8
-8.00	0.1	0	0	8
-9.00	0.2	0	0	8
-9.50	0.2	0	0	8
-9.70	Breakdown, attractor to needle			
		P_0 = 200 psig		
-8.00	0.2	0	0	10
-9.00	0.3	0	0	10
-10.0	0.4	0	0	10
-11.0	0.4	0	0	10
-11.5	0.4	0	0	10
-11.7	0.4	0	7	10
-12.0	0.4	0	20	10
-12.0	Breakdown, attractor to needle			

TABLE X

Current Characteristic Data, Configuration VI
(L = 0.50 inch)

V_a	I_a	I_{gp}	I_c	T_0
		P_0 = 100 psig		
-5.00	0.0	0	0	-7
-6.00	0.1	0	13	-7
-6.50	0.1	1	15	-7
-7.00	0.1	1	16	-7
-7.30	0.1	1	16	-7
-7.50	Breakdown, attractor to needle			
		P_0 = 150 psig		
-6.50	0.0	0	0	-6
-7.00	0.0	0	7	-5
-8.00	0.0	1	18	-5
-8.50	0.0	2	48	-6
-9.00	0.0	5	90	-6
-9.50	0.1	6	106	-6
-9.70	0.1	8	108	-6
-10.0	Breakdown, attractor to needle			
		P_0 = 200 psig		
-6.00	0.0	0	0	-4
-7.00	0.0	0	2	-4
-8.00	0.0	0	23	-4
-9.00	0.0	2	68	-4
-10.0	0.0	6	152	-4
-11.0	0.0	11	218	-4
-11.7	0.1	20	325	-4
-11.9	Breakdown, attractor to needle			

TABLE XI

Current Characteristic Data, Configuration VII
(L = 0.50 inch)

V_a	I_a	I_{gp}	I_c	T_0
		P_0 = 100 psig		
-4.00	0.0	0	0	5
-5.00	0.0	0	5	6
-5.50	0.1	1	34	6
-6.00	0.2	2	40	7
-6.50	0.5	9	81	8
-7.00	1.5	23	123	8
-7.00	Breakdown, attractor to needle			
		P_0 = 150 psig		
-6.50	0.0	0	0	9
-7.00	0.0	0	2	9
-8.00	0.4	3	64	9
-8.50	1.8	27	210	9
-9.00	2.0	58	280	9
-9.50	2.4	92	325	9
-10.0	3.0	114	345	9
-10.5	4.0	160	360	9
-10.5	Breakdown, attractor to needle			
		P_0 = 200 psig		
-6.50	0.0	0	0	10
-7.00	0.0	0	4	10
-8.00	0.5	1	57	10
-9.00	2.8	14	230	10
-10.0	4.0	39	345	10
-11.0	5.0	75	425	10
-12.0	6.4	153	480	10
-13.0	7.0	240	500	10
-13.0	Breakdown, attractor to ground plate			

TABLE XII

Current Characteristic Data, Configuration VIII
(L = 0.50 inch)

V_a	I_a	I_{gp}	I_c	T_o
		P_o = 100 psig		
-5.00	0.2	2	54	-14
-6.00	1.2	24	150	-15
-7.00	15	125	248	-15
-8.00	94	250	272	-15
-8.50	195	300	270	-15
-9.00	350	330	267	-15
-9.27	500	340	257	-15
-9.27	Breakdown, attractor to ground plate			
		P_o = 150 psig		
-6.00	0.0	0	9	-14
-7.00	1.2	1	57	-14
-8.00	4.5	30	232	-14
-9.00	7.2	114	355	-14
-10.0	25	225	400	-14
-10.5	40	260	400	-14
-10.5	Breakdown, attractor to ground plate			
		P_o = 200 psig		
-6.00	0.1	0	22	-19
-7.00	1.3	1	61	-19
-8.00	5.5	10	204	-19
-9.00	7.5	40	350	-18
-10.0	9.0	80	420	-17
-11.0	10	123	455	-16
-11.0	Breakdown, attractor to ground plate			

TABLE XIII

Current Characteristic Data, Configuration IX
(L = 0.50 inch)

V_a	I_a	I_{gp}	I_c	T_0
		P_0 = 100 psig		
-4.00	0.0	0	0	-16
-4.50	0.0	1	17	-17
-5.00	0.3	5	45	-17
-5.50	1.4	29	103	-17
-6.00	7.8	106	168	-17
-6.50	30	200	220	-17
-7.00	89	270	225	-17
-7.50	190	310	225	-17
-8.00	340	330	225	-17
-8.44	500	340	225	-17
		(No breakdown)		
		P_0 = 150 psig		
-5.00	0.2	0	0	-16
-6.00	0.4	1	27	-16
-6.50	1.2	7	88	-16
-7.10	3.1	35	200	-16
-8.00	7.5	136	300	-16
-8.60	20	230	325	-16
-9.30	55	320	340	-16
-10.0	130	420	340	-16
-10.2	Breakdown, attractor to ground plate			
		P_0 = 200 psig		
-5.00	0.6	0	0	-14
-6.00	0.8	0	22	-14
-7.00	2.5	3	77	-15
-7.50	5.0	15	180	-15
-8.00	7.5	30	254	-15
-8.50	9.5	60	310	-15
-9.00	11	93	360	-15
-9.50	14	130	390	-15
-10.0	16	180	410	-15
-10.2	Breakdown, attractor to ground plate			

TABLE XIV

Current Characteristic Data, Configuration X
(L = 0.50 inch)

V_a	I_a	I_{gp}	I_c	T_0
		P_0 = 100 psig		
-4.00	0.0	0	0	-27
-4.50	0.1	1	13	-28
-5.00	0.3	3	31	-28
-5.50	2.3	16	94	-28
-6.00	8.8	52	163	-28
-6.50	30	110	210	-27
-7.00	76	169	226	-27
-7.50	136	200	231	-26
-8.00	230	220	232	-26
-8.50	350	240	235	-26
-9.00	485	250	236	-26
-9.10	500	250	235	-25
		(No breakdown)		
		P_0 = 150 psig		
-5.00	0.0	0	0	-22
-6.00	0.0	0	5	-22
-7.00	1.5	4	55	-22
-7.50	4.0	18	136	-21
-8.00	7.8	59	230	-20
-8.50	19	119	282	-20
-9.00	44	184	310	-20
-9.50	76	230	325	-19
-10.0	87	240	330	-18
-10.5	130	260	330	-18
-11.0	210	300	335	-18
-11.0	Breakdown, attractor to ground plate			
		P_0 = 200 psig		
-6.00	0.0	0	0	-18
-7.00	0.0	1	22	-18
-8.00	3.5	14	148	-18
-9.00	8.0	77	310	-18
-10.0	19	163	365	-18
-10.5	26	175	375	-18
-11.0	51	245	395	-18
-11.0	Breakdown, attractor to ground plate			

TABLE XV

Data Showing Effect of Variation of Total Pressure
(Configuration VII, L = 0.50 inch)

P_o	$V_{a\ max}$	I_a	I_{gp}	I_c	I_n	T_o
80	-5.8	2.8	13	55	85	17
100	-7.0	2.0	34	117	175	18
120	-8.4	3.0	62	200	300	19
140	-9.3	9.0	115	320	480	20
160	-10.7	11.0	150	415	630	21
180	-11.2	4.0	140	465	670	24
200	-11.7	2.0	130	515	710	25
220	-12.1	2.0	110	540	735	26
240	-12.4	0.8	100	570	750	27

Note: From $P_o = 80$ through $P_o = 160$, $V_{a\ max}$ was limited by breakdown from the attractor to the needle. Above $P_o = 160$, $V_{a\ max}$ was limited by breakdown from the attractor to the ground plate.

TABLE XVI

Data Showing Effect of Length of Transport Region
(Configuration VII)

L	V_a max	I_a	I_{gp}	I_c	I_n	T_o
			P_o = 150 psig			
1/8	-8.35	1	6	253	295	40
1/4	-8.30	3	16	275	325	41
1/4	-8.35	1	12	270	320	39
3/8	-8.30	3	19	240	300	40
1/2	-8.20	2	35	240	310	40
5/8	-8.25	2	55	230	320	39
3/4	-8.25	2	83	215	335	42
7/8	-8.30	2	100	180	320	44
1	-8.35	2	128	133	300	41
			P_o = 200 psig			
1/8	-10.5	1	9	525	585	40
1/8	-10.4	3	12	500	575	42
1/4	-10.4	1	22	520	600	42
1/4	-10.3	3	26	480	560	44
3/8	-10.2	1	37	500	590	42
1/2	-10.2	2	65	455	575	42
5/8	-10.2	2	95	430	575	43
3/4	-10.2	2	160	365	575	44
7/8	-10.3	2	200	310	565	44
1	-10.2	1	250	263	570	42

TABLE XVII

Data for Comparison of Positive and Negative Ion Flows: Positive Flow
(Configuration VII, L = 0.50 inch)

V_a	I_a	I_{gp}	I_c	I_n	T_0
		P_0 = 100 psig			
-4.10	0.0	0	0	0	35
-4.30	0.0	0	13	20	37
-4.50	0.0	1	21	30	38
-4.80	0.0	2	26	37	38
-5.20	0.0	4	40	54	38
-5.70	0.0	6	46	61	39
-5.90	0.0	8	62	81	39
-6.10	0.1	11	76	98	39
-6.35	1.0	14	77	106	39
-6.35	Breakdown, attractor to needle				
		P_0 = 150 psig			
-5.20	0.0	0	0	0	40
-5.70	0.0	0	18	28	41
-6.46	0.0	3	38	55	41
-7.00	0.0	7	70	95	42
-7.35	0.0	13	107	144	42
-7.60	0.1	21	159	206	42
-7.92	0.2	32	212	276	42
-8.00	Breakdown, attractor to needle				
		P_0 = 200 psig			
-6.00	0.0	0	0	0	42
-6.60	0.0	0	14	22	42
-7.20	0.1	2	42	63	43
-7.80	0.1	5	67	95	43
-8.15	0.1	12	157	204	44
-8.50	0.1	20	210	270	44
-9.00	0.4	39	300	385	44
-9.20	0.5	48	375	470	44
-9.20	Breakdown, attractor to needle				

TABLE XVIII

Data for Comparison of Positive and Negative Ion Flows: Negative Flow
(Configuration VII, L = 0.50 inch)

V_a	I_a	I_{gp}	I_c	I_n	T_0
		P_0 = 100 psig			
+3.60	0.0	0	0	0	42
+4.00	0.0	0	3	5	42
+4.51	0.0	1	12	16	42
+5.00	0.1	5	35	47	43
+5.50	0.6	13	65	90	43
+6.00	3.2	31	112	160	43
+6.30	7.0	50	156	225	43
+6.40	Breakdown, attractor to needle				
		P_0 = 150 psig			
+5.50	0.0	0	0	0	44
+6.00	0.0	0	8	12	45
+6.50	0.0	3	45	60	46
+7.00	0.1	14	98	130	46
+7.50	0.4	36	226	285	46
+8.00	1.0	50	280	360	46
+8.15	1.5	60	295	390	46
+8.25	2.8	70	300	410	46
+8.25	Breakdown, attractor to needle				
		P_0 = 200 psig			
+6.00	0.0	0	7	10	51
+6.50	0.0	1	31	45	51
+7.00	0.0	3	68	90	51
+7.50	0.1	13	168	210	51
+8.00	0.1	31	300	375	51
+8.50	0.2	50	390	480	52
+9.00	0.3	65	430	540	52
+9.50	0.5	90	450	580	52
+10.0	2.0	90	460	600	52
+10.0	Breakdown, attractor to needle				

Vita

Terry N. Lauritsen, son of William H. Lauritsen and Francel M. Lauritsen, was born on [redacted]. He was valedictorian of the class of 1952 at Helix High School, La Mesa, California, and then entered San Diego State College, San Diego, California. In June, 1956, he was graduated with the degree of Bachelor of Science in Engineering, with Highest Honors, and with Distinction in Engineering and in Air Science. He was employed as an Aerodynamics Engineer at Convair Astronautics for six months prior to entering active duty as an officer in the Regular United States Air Force. He served four years at Edwards Air Force Base, California, with duty as a mechanical engineer, and was then, in the summer of 1960, assigned to the Institute of Technology.

Permanent address: [redacted]

This thesis was typed by Marjorie M. Keppler.